Tribology of NiCrAlY+Al_2O_3 composite coatings by plasma spraying with hybrid feeding of dry powder+suspension

G. Bolelli, A. Candeli, L. Lusvarghi, A. Ravaux, K. Cazes, A. Denoirjean, S. Valette, C. Chazelas, E. Meillot, L. Bianchi

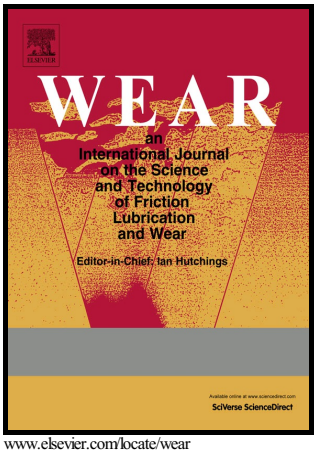

www.elsevier.com/locate/wear

PII: S0043-1648(15)00459-7
DOI: http://dx.doi.org/10.1016/j.wear.2015.10.014
Reference: WEA101526

To appear in: *Wear*

Received date: 3 June 2015
Revised date: 19 October 2015
Accepted date: 25 October 2015

Cite this article as: G. Bolelli, A. Candeli, L. Lusvarghi, A. Ravaux, K. Cazes A. Denoirjean, S. Valette, C. Chazelas, E. Meillot and L. Bianchi, Tribology o NiCrAlY+Al_2O_3 composite coatings by plasma spraying with hybrid feeding o dry powder+suspension, *Wear,* http://dx.doi.org/10.1016/j.wear.2015.10.014

Tribology of NiCrAlY + Al_2O_3 composite coatings by plasma spraying with hybrid feeding of dry powder + suspension

G. Bolelli[1*], A. Candeli[1], L. Lusvarghi[1], A. Ravaux[2], K. Cazes[2], A. Denoirjean[2], S. Valette[2], C. Chazelas[2], E. Meillot[3], L. Bianchi[3]

[1] Department of Engineering "Enzo Ferrari", University of Modena and Reggio Emilia, Via P. Vivarelli 10/1, 41125 Modena (MO), Italy

[2] SPCTS –European Ceramics Center, 12, Rue Atlantis, 87068 Limoges Cedex, France

[3] CEA Le Ripault, Laboratoire de Projection Thermique, BP 16, 37260 Monts, France

* Corresponding author: tel. 0039 0592056233; fax: 0039 0592056243;

e-mail: giovanni.bolelli@unimore.it

Abstract

NiCrAlY layers containing different amounts of Al_2O_3 (0, 3, 6, 12, 18 wt.%) were deposited onto stainless steel substrates by a "hybrid" plasma spray process whereby the NiCrAlY powder was fed in dry form whilst fine Al_2O_3 powder, dispersed in ethanol, was injected through a suspension feeding system.

The Al_2O_3 reinforcement, consisting of fine, rounded particles interspersed within larger NiCrAlY lamellae, only causes marginal changes in hardness, due to the limited particles-matrix cohesion. Nonetheless, at room temperature, ball-on-disk dry sliding wear rates against sintered Al_2O_3 counterparts decrease from $\approx 5*10^{-4}$ $mm^3/(Nm)$ for pure NiCrAlY to $\approx 5*10^{-6}$ $mm^3/(Nm)$ with 18 wt.% Al_2O_3 addition. Pure NiCrAlY indeed suffers adhesive wear, whereas, on the composite coatings, the pull-out of some Al_2O_3 particles triggers the formation of a tribo-layer of smeared oxide fragments, which mediates the contact with the counterbody.

At 400 °C and at 700 °C, all wear rates are levelled to $\approx 8*10^{-5}$ $mm^3/(Nm)$ and $\approx 2*10^{-5}$ $mm^3/(Nm)$, respectively. An oxide layer grows on the NiCrAlY matrix upon high-temperature exposure,

resulting in a tribo-oxidation wear mechanism, which makes the addition of Al_2O_3 irrelevant. At 700 °C, coatings are further strengthened by partial healing of interlamellar defects and by fine-grained β-NiAl precipitating within the metal matrix.

Keywords: Sliding wear; High temperature; Thermal spray coatings; Metal-matrix composite; Electron microscopy.

1. Introduction

Thick coatings for the long-term protection of mechanical components against severe sliding wear at high temperatures are needed in a variety of important industrial applications, foremost of which is the energy production field. Examples include the protection of shafts and bearings in aeronautical and land-based gas turbines [1], of steam turbine parts [2] and of components for nuclear power plants [3–5], etc.

Presently, however, there is no fully established solution to this need. Hardmetals, particularly those based on chromium carbides (e.g. Cr_3C_2-NiCr), are quite widely used [1–4], but they present some disadvantages. Due to their high hardness, machining of these coatings is time-consuming and expensive. They also possess non-optimal oxidation resistance at the highest temperatures, due to inward oxygen diffusion through the chromium carbide particles and, consequently, to their selective degradation [6].

Better performances in oxidising environments would be achieved with systems based on MCrAlY-type alloys (where M = Co and/or Ni), which are accordingly employed to prevent oxidation and hot corrosion of turbine blades, vanes, and of other components in the hot sections of gas turbines, up to ≈1100 °C [7]. Pure MCrAlYs, however, are unsuitable for tribological applications, because their low hardness would result in very severe wear under sliding contact conditions, particularly

during running-in stages at low temperatures. Literature studies on this topic have indeed reported significant wear by adhesion and delamination mechanisms under rotating and oscillating sliding [8–10].

The manufacturing of composite coatings based on MCrAlY alloys reinforced by refractory oxides (e.g. Al_2O_3) therefore appears as a viable solution in order to couple the oxidation resistance of the metal matrix to the hardness and chemical stability of the ceramic phase [2,11–14]. In most of the cited references, such MCrAlY+Al_2O_3 composites were deposited by thermal spray processes: their main advantages include high productivity and flexible coupling of a large variety of coating and substrate materials [15]. They are indeed the standard choice for the deposition of oxidation-resistant MCrAlY alloys in the above-mentioned gas turbine applications [7].

One way to deposit thermally-sprayed MCrAlY+Al_2O_3 composite coatings can be that of using a composite feedstock powder, which can be obtained e.g. by mechanical alloying via high-energy ball-milling of MCrAlY and Al_2O_3 powders. Some literature concerning the sliding wear behaviour of such thermally sprayed MCrAlY+Al_2O_3 mechanically alloyed composites accordingly exists [12,13], although, in all of the cited references, only one test temperature was employed, whilst a systematic tribological study is not yet available. The high-energy ball milling approach has also been investigated in detail for the production of bond coating systems in thermal barrier coatings, as the thermal expansion coefficient of MCrAlY+Al_2O_3 composites is intermediate between that of an underlying pure MCrAlY layer and that of a Y_2O_3-stabilised ZrO_2 thermally insulating top coat [16,17]. In this case, however, no tribological studies have been carried out yet. A chemical reaction process, involving the hydrogen reduction of a Ni salt in a mixture comprising Co, Cr, Al, Y_2O_3, Al_2O_3 and B_4C, followed by agglomeration and sintering, has also been employed recently to produce composite MCrAlY+Al_2O_3/B_4C powders [14].

Another highly innovative way to obtain such composite coatings is to employ a “hybrid” approach based on the recently introduced suspension thermal spray processes [18], whereby a thermal spray apparatus (and, in particular, its feedstock handling and injection system) is modified in order to

process suspensions of fine particles dispersed in a liquid carrier [19]. The liquid carrier indeed confers adequate flowability and momentum to sub-micrometric particles, enabling their delivery into the core of a hot gas stream [19,20]. Conventional feeding systems, which employ a gas carrier, can instead process feedstock powders with particle sizes of the order of some tens of micrometres only [21]. In particular, suspension injection would be highly advantageous to process the Al_2O_3 reinforcement, which should have very fine particle size. The MCrAlY matrix, on the other hand, is more conveniently sprayed by a conventional approach, in order to avoid the excessive oxidation that would affect an extremely fine metal powder heated in an oxygen-containing environment (such as that of a thermal plasma jet expanding into air).

Therefore, a hybrid, dual-feed plasma spray system, simultaneously equipped with a conventional dry powder feeder and with a suspension injector, is employed in this study in order to deposit MCrAlY+Al_2O_3 composites with various Al_2O_3 contents. Very few literature reports are available where a similar hybrid approach has been employed [22]. Its advantage lies in the fact that it avoids the need for powders pre-alloying, which reduces the complexity and cost of feedstock preparation. On the other hand, the dispersion of the Al_2O_3 phase will not be as homogeneous as it would be with ball-milled powders, since the reinforcing Al_2O_3 particles can only be located between MCrAlY lamellae and not inside them.

This paper particularly focuses on the dry sliding wear behaviour of coatings containing various amounts of Al_2O_3 (0, 3, 6, 12, 18 wt.%), tested at three different temperatures (room temperature, 400 °C, 700 °C). Microstructure, phase composition and micro-mechanical properties are also studied in order to assist the tribological interpretation.

2. Experimental

2.1 Samples manufacturing

All samples were manufactured by atmospheric plasma spraying using a TriplexPro-200 torch (Oerlikon-Metco, Wohlen, Switzerland) featuring three cathodes and a single anode nozzle.

The feedstock for the MCrAlY matrix was a commercially available gas-atomised Ni – 22wt.%Cr – 10wt.%Al – 1wt.%Y powder (AMDRY 9624, Oerlikon-Metco), with -45+15 μm nominal particle size distribution, which was conventionally fed to the torch in dry form. The powder injector, having a 1.5 mm-diameter nozzle, was placed 1 cm downstream of the anode nozzle exit and was oriented perpendicularly to the torch axis.

The feedstock for the Al_2O_3 reinforcement was a sub-micrometric powder (AKP-30, Sumitomo Chemicals Co., Japan), with average particle size of 300 nm. As these fine particles would have insufficient flowability and insufficient momentum to allow conventional injection into the plasma stream using a gas carrier, the powder was dispersed in ethanol medium with the aid of 2 wt.% dispersant (Beicostat C213) and fed using a liquid delivery system based on pressurised liquid reservoirs. The suspension is delivered through an injector having a sapphire nozzle with 150 μm diameter. The injector is inclined at 70° with respect to the torch axis and placed in such a way, that the suspension stream is directed towards the centre of the anode nozzle exit.

A schematic of the torch set-up, with photographs of the plasma plume, is provided in Fig. 1.

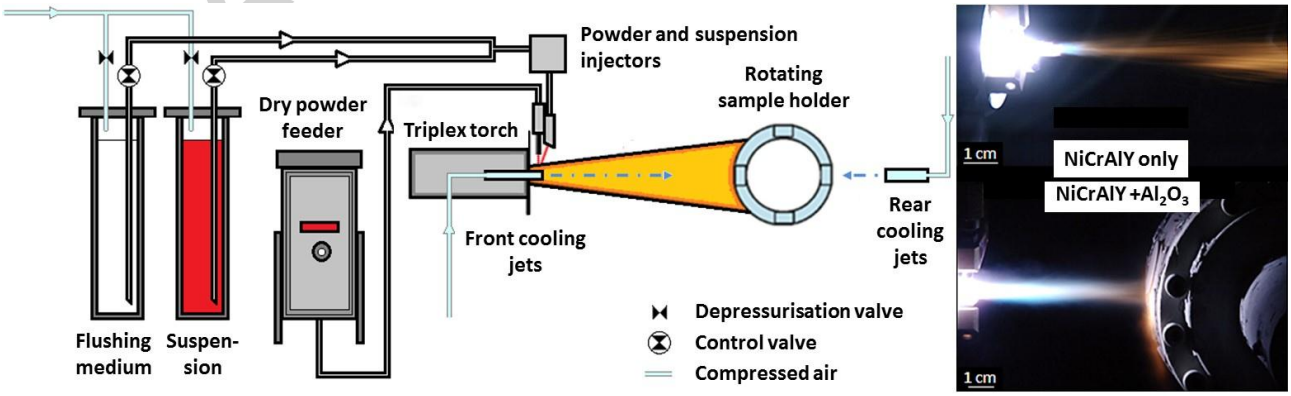

Figure 1. Schematics of the "hybrid" plasma spray set-up and photographs of the plasma plume with powder and powder + suspension injection.

The TriplexPro-200 torch allows adjusting the circumferential location of the injector relative to the position of the three plasma lobes issuing out of the three cathodes. Preliminary diagnostic tests using a shadowgraphic technique (with a set-up similar to the one described in [23]), however, showed that the circumferential position of the suspension injector produces no visible effect on the injected suspension stream. Injection locations were therefore selected so that the suspension was delivered in the position of a plasma lobe while the powder was delivered in between two lobes. This should ensure full treatment of the Al_2O_3 particles while preventing overheating of the metal powder (which would result in excessive oxidation). The complete list of process parameters is provided in Table I.

In order to change the relative amounts of NiCrAlY matrix and Al_2O_3 reinforcement in the coatings, the feed rate of the NiCrAlY powder and the solid content of the suspension were varied as listed in Table II. To the contrary, the flow rate of the gas carrier for the dry metal powder and the pressure in the suspension reservoir were kept constant at the pre-determined optimal values (Table I).

Table I. Plasma spray process parameters.

TORCH SETTINGS	*Anode nozzle diameter [mm]*	6.5
	Current [A]	450
	Voltage [V]	103.4
	Primary gas type / flow rate (SL/min)	Ar /70
	Plasma enthalpy [MJ/kg]	12.8
	Stand-off distance [mm]	100
	Substrate pre-heating temperature [°C]	200 – 250
	N° of pre-heating cycles	20
SYSTEM KINEMATICS	*Torch-substrate relative speed [m/s]*	1
	Pass spacing [mm]	10
	N° of deposition cycles	67
INJECTION SETTINGS	*Powder injector diameter [mm]*	1.8
	Powder feed rate [g/min]	10 – 35
	Feeding gas flow rate [SL/min]	7
	Suspension injector diameter [μm]	150
	Injection pressure [MPa]	0.6
	Solid content in the suspension (wt.%)	10 – 40
	Suspension feed rate [mL/min]	30

Table II. Powder feed rates and suspension concentrations for the various deposition experiments.

Nominal composition [wt.%]	Actual content of Al_2O_3 [wt.%]	Solid content in the suspension [wt.%]	Dry powder feed rate [g/min]
NiCrAlY	0	-	20
NiCrAlY+3%Al_2O_3	3.4	10	35
NiCrAlY+6%Al_2O_3	5.9	10	20
NiCrAlY+12%Al_2O_3	12.1	20	10
NiCrAlY+18%Al_2O_3	17.6	40	10

2.2 Wear testing

The wear resistance of the samples was studied under dry sliding conditions by unidirectional rotating ball-on-disk testing following the ASTM G99 standard (High Temperature Tribometer, Anton Paar TriTec, Peseux, Switzerland). This test has accordingly been frequently used to characterise the sliding wear behaviour of similar MCrAlY-type coatings at various temperatures [11,13,24,25].

The goal of the present test was to screen out the performances of the various coatings as a function of temperature and of their Al_2O_3 content, and to provide a general understanding of their fundamental sliding wear behaviour. For this purpose, sintered Al_2O_3 balls of 6 mm diameter were chosen as the counterbody. Due to their chemical inertness, they do not elicit unwanted tribochemical interactions with the coating material, which would interfere with the "intrinsic" behaviour of the latter and confuse the interpretation of processes such as tribo-oxidation and tribofilm formation. Such counterpart is also suitable to simulate the frequent circumstance in which wear is caused by the presence of hard asperities in the tribosystem (e.g. hard oxidised debris formed in-situ or transported from other areas of an industrial machinery, hard phases in the counterbody material, hard oxidised asperities due to tribo-oxidation, etc.).

Tests were performed over a 2000 m sliding distance, with a relative sliding speed of 0.10 m/s and a wear track radius of 5 mm, under a normal load of 5 N. The tests were run at room temperature (≈25 °C), at 400 °C and at 700 °C, in order to cover a broad range of temperatures relevant to a

large variety of potential applications. Moreover, the indications of the tests are useful to predict the behaviour of the coatings during low-temperature run-in stages, which may occur in some applications (e.g. gas turbine shaft bearings – see the Introduction) before reaching the operational temperature.

In high temperature tests, the ball-on-disk system was induction-heated from the base plate and the temperature of the sample was monitored using a thermocouple in contact with its backside. The sample was heated to the prescribed temperature in approximately 1 h and was left in isothermal conditions for another 40 min before the test was commenced, in order to homogenise the system temperature. This means the samples remained at the operating temperature for an overall duration of ≈6 h 10 min before natural cooling.

The samples were ground and polished to Ra ≈ 0.02 μm, and ultrasonically cleaned in acetone before testing. The friction coefficient was measured during the test using a load cell; the volume loss of the sample was obtained by acquiring the profile of the wear track with an optical confocal profilometer (Conscan profilometer, Anton Paar TriTec) and that of the counterpart was determined by measuring the diameter of the worn cap by optical microscopy. Wear rates were obtained as the volume loss per unit normal load and unit sliding distance. On-line monitoring of the vertical displacement of the ball holder provided further, qualitative assessment of the overall system wear (sample + ball counterpart altogether) at room temperature. The measurement is not usable at high temperature due to the additional effect of thermal expansion of the ball holder on the vertical position.

The worn surfaces of the samples were inspected with a field emission gun (FEG) – scanning electron microscope (SEM: Nova NanoSEM 450, FEI, Eindhoven, The Netherlands) equipped with energy-dispersive X-ray (EDX) microanalysis (Quantax-200, Bruker). The loose wear debris collected onto the samples after each test was also analysed by SEM (Quanta-200, FEI) + EDX microanalysis (Inca, Oxford Instruments Analytical, Abingdon, UK) and its phase composition was

analysed by micro-Raman spectroscopy (LabRam, Horiba Jobin-Yvon, Villeneuve D'Ascq, France) using a 632.81 nm-wavelength He:Ne laser focussed through a 100x objective.

2.3 Microstructural and phase analyses

The cross-sectional morphologies of the samples, both in as-deposited conditions and after testing at 400 °C and 700 °C, were observed by FEG-SEM. The samples were cold-mounted in epoxy resin, metallographically cut, ground with diamond papers (up to 1200 mesh size), polished with 3 µm diamond slurry and with a colloidal silica suspension, and ultrasonically cleaned in isopropanol before observation. The same procedure was also employed in order to characterise the cross-section of the NiCrAlY feedstock powder.

Microhardness and elastic modulus were measured on these polished cross-sections by depth-sensing Berkovich micro-indentation (Micro-Combi Tester, Anton Paar TriTec) using a maximum applied load of 3 N (suitable to measure the overall properties of the coating, as shown in [26]), a holding time of 15 s at maximum load, and a loading/unloading rate of 4.5 N/min. The Oliver-Pharr procedure [27] was employed in accordance with ISO 14577. All results were expressed as average ± standard deviation of 20 usable indentations. Those presenting very large cracks upon optical microscopy inspection, and/or those presenting obvious pop-in events in the load-penetration curves were discarded.

The phase composition of the samples was assessed by X-ray diffraction (XRD: X'Pert PRO, PANAlytical, Almelo, The Netherlands) using Ni-filtered Cu-Kα radiation emitted from a tube operated at 40 kV, 40 mA.

The exact amount of Al_2O_3 contained in the coatings was determined by X-ray fluorescence (XRF: ARL SMS-Omega, Thermo Scientific, Waltham, MA, USA). Assuming that vaporisation of elements from the matrix does not take place to a significant extent during plasma spraying, the ratio between the amounts of Al, Cr, Ni and Y in the original feedstock powder is employed to

determine which fraction of Al in the analysis of the coatings is due to the matrix. The amount of Al_2O_3 is therefore computed from the remaining part of the Al contained in the coating.

3. Results and discussion

3.1 Microstructure and phase composition – as-deposited coatings

The as-deposited coatings (Fig. 2) exhibit dense microstructures with some porosity (Fig. 2 – circles). Some of the micrographs also show the Berkovich micro-indentation marks (Fig. 2C – square mark). See Section 3.3 for a discussion on the latter.

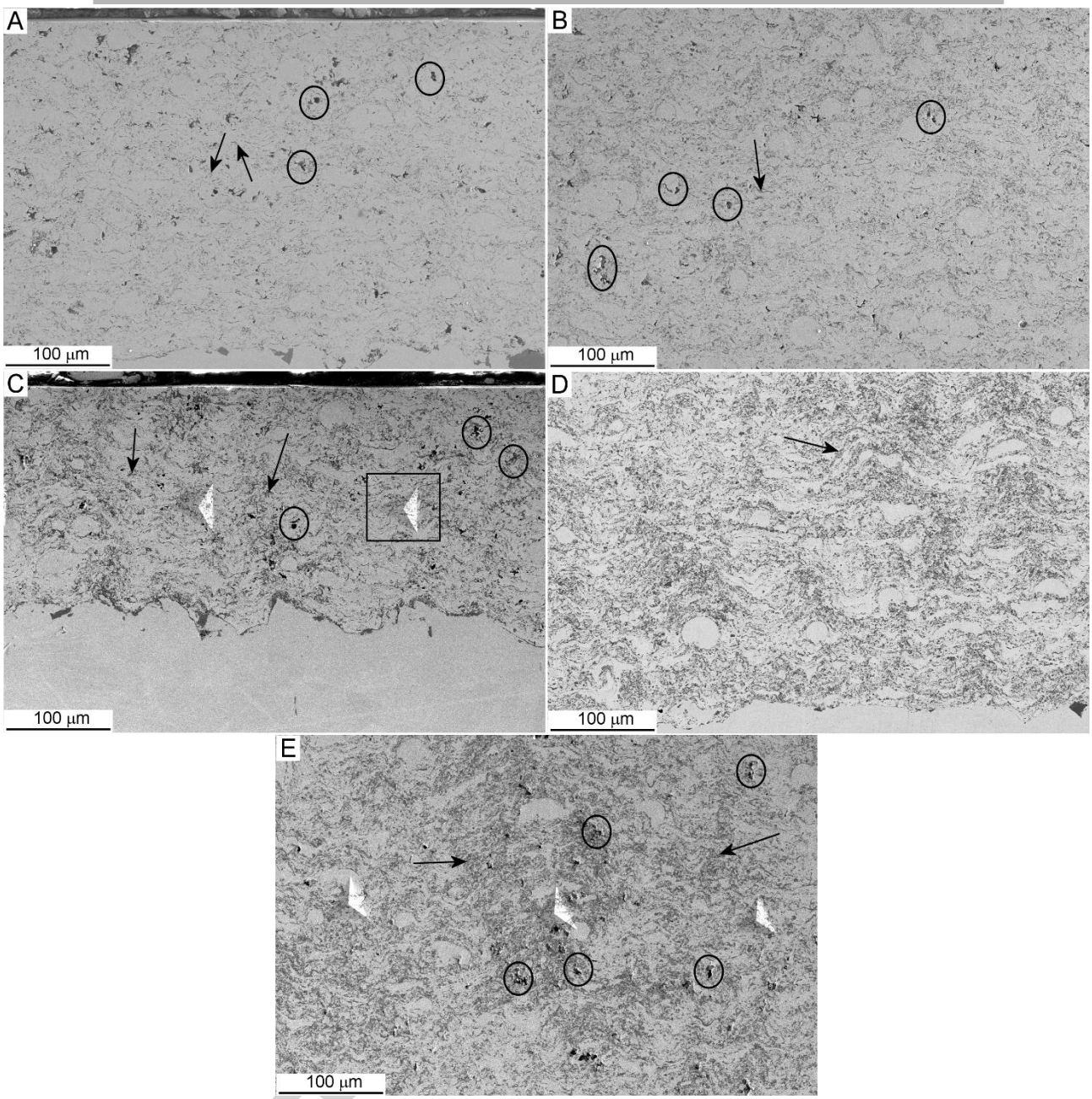

Figure 2. Cross-sectional FEG-SEM micrographs of the NiCrAlY coatings containing (A) 0 wt.%, (B) 3 wt.%, (C) 6 wt.%, (D) 12 wt.% and (E) 18 wt.% Al_2O_3.
Circles = pores; Square = Berkovich indentation mark; Arrows = oxides.

As the amount of Al_2O_3 co-deposited with the NiCrAlY powder increases, the overall amount of oxide phases contained in the coatings (recognisable by their darker contrast in the backscattered electron SEM micrographs of Fig. 2 – some are marked by arrows for better clarity) obviously grows. Two distinct types of oxides can indeed be discerned (Fig. 3A,B), one returning a slightly brighter contrast (label 1) whilst the other one provides the darkest contrast (label 2). The brighter oxide phase contains Al and Y together with some Cr and Ni (Fig. 3C – spectrum 1). This phase is

therefore contributed by the oxidation of NiCrAlY particles (amorphous Al,Y-rich oxide stringers were accordingly identified in MCrAlY coatings by TEM analysis in [28]), which may occur either during the flight period or immediately after impact, as shown in detail in [29]. On the other hand, the darkest oxide phase consists of the Al_2O_3 reinforcement particles (Fig. 3C – spectrum 2). Only very weak peaks of Ni, probably coming from a moderate contribution of the surrounding material, are indeed identifiable in their EDX spectra.

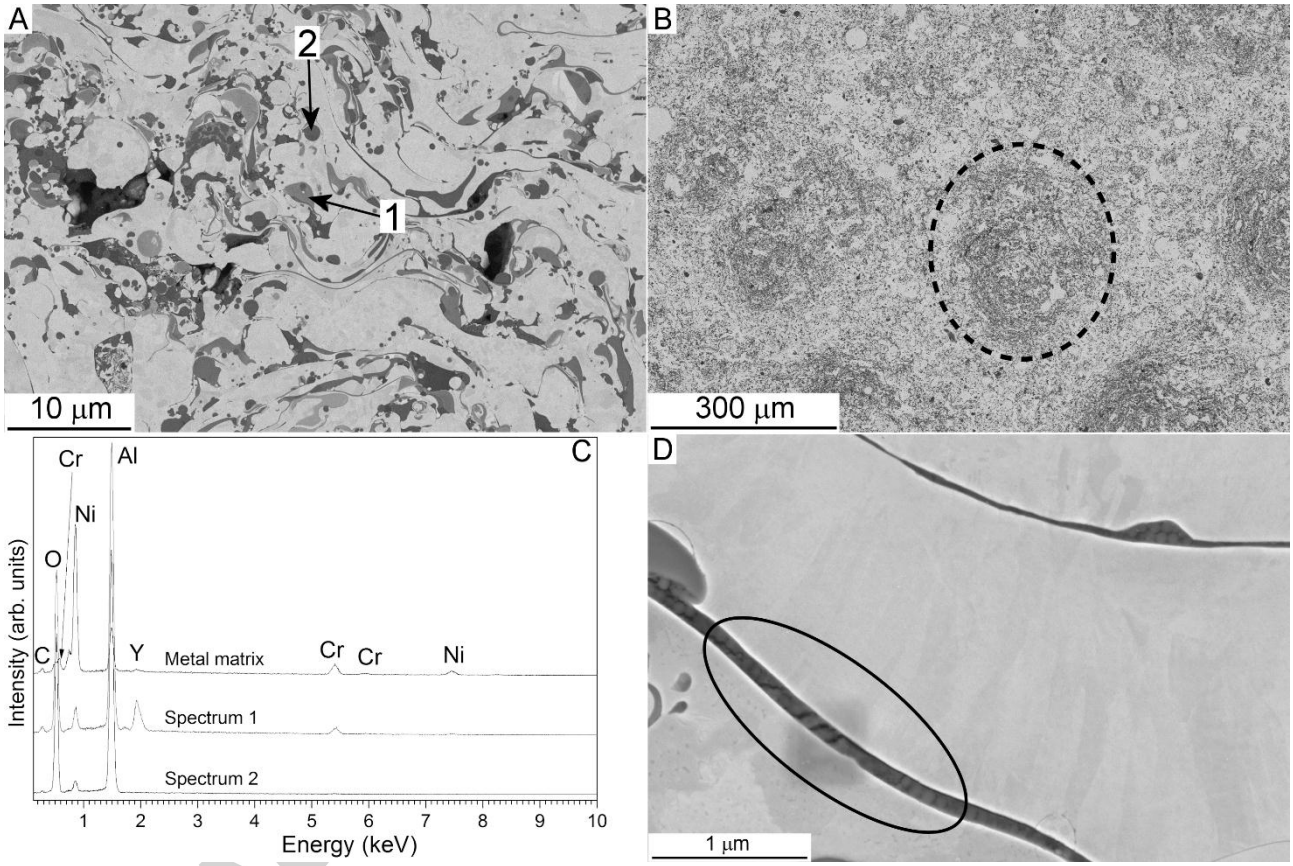

Figure 3. Backscattered electron FEG-SEM micrographs of the cross-section of the NiCrAlY + 3 wt.% Al_2O_3 sample (A) and of the polished top surface (B) of the NiCrAlY + 18 wt.% Al_2O_3 sample, with EDX microanalysis (C) of the areas indicated in panel A. Detail of a microcracked oxide inclusion (circled area) along the boundary between adjacent NiCrAlY lamellae in the NiCrAlY + 6 wt.% Al_2O_3 coating (D).

Quantification of the Al_2O_3 content via image analysis from such micrographs would be quite unreliable: it is difficult to tell the Al_2O_3 reinforcement from oxidised NiCrAlY, due to the limited difference between their greyscale contrast levels. XRF quantification of the overall amount of Al is

therefore a much more reliable way to determine the actual content of Al_2O_3 in the samples. The results are shown in Table II.

Oxidation is an undesirable, yet unavoidable phenomenon during the processing of NiCrAlY alloys by atmospheric plasma spraying [30]. It deprives the metal matrix of aluminium and yttrium, i.e. the most reactive elements, which are primarily responsible for the formation of protective oxide scales at high temperatures [30–33]. Moreover, these oxides weaken the interlamellar boundary by forming elongated stringers, which prevent metal-to-metal adhesion causing local brittleness. Thermal shocks, such as those caused by the rapid cooling upon impact or by the thermal cycles during subsequent passes of the torch over pre-deposited coating layers, can indeed pre-crack these oxide stringers (Fig. 3D - circle). These features shall have a direct effect on the mechanical and tribological properties of the system as detailed in Sections 3.3 and 3.4.

The added Al_2O_3 particles, on the other hand, mostly appear as quite rounded inclusions (Fig. 3A,B), so that they will not have the same negative effect on interlamellar quality. Such rounded shape is due to the rather low temperature and velocity which these particles, replicating the gas flow characteristics because of their low inertia (low Stokes number), acquire in the vicinity of the substrate [34–37]. Plasma spraying with pure suspensions indeed requires much shorter stand-off distances than conventional plasma-spraying of large, dry powders [18,19]. In the present case, however, long distances are required both because the NiCrAlY powder needs to be properly melted and accelerated, and because flattening of the Al_2O_3 particles would not really be desirable. In order to exert its reinforcing action, indeed, Al_2O_3 should appear as uniformly dispersed particles, rather than as elongated inclusions between the NiCrAlY lamellae, otherwise they would cause interlamellar embrittlement just as the in-flight oxides do.

When the Al_2O_3 amount is high (hence particularly in the coating containing 18 wt.% Al_2O_3), however, the particles do not distribute homogeneously, but tend to cluster (Figs. 2E and 3B: one such cluster is marked by the dashed circle). This resembles the formation of the well-known

"columnar" or "cone-shaped" features frequently described in suspension sprayed coatings [37]. The cause is the stagnation flow in front of the substrate: it deflects the fine Al_2O_3 particles, due to their low inertia, conferring them a velocity component parallel to the substrate surface. The deflected particles have greater chance to stick to some protruding peak [37]. At some locations, the deposition rate of Al_2O_3 particles is therefore higher than in others, resulting in the typical cluster morphologies of Figs. 2E and 3B.

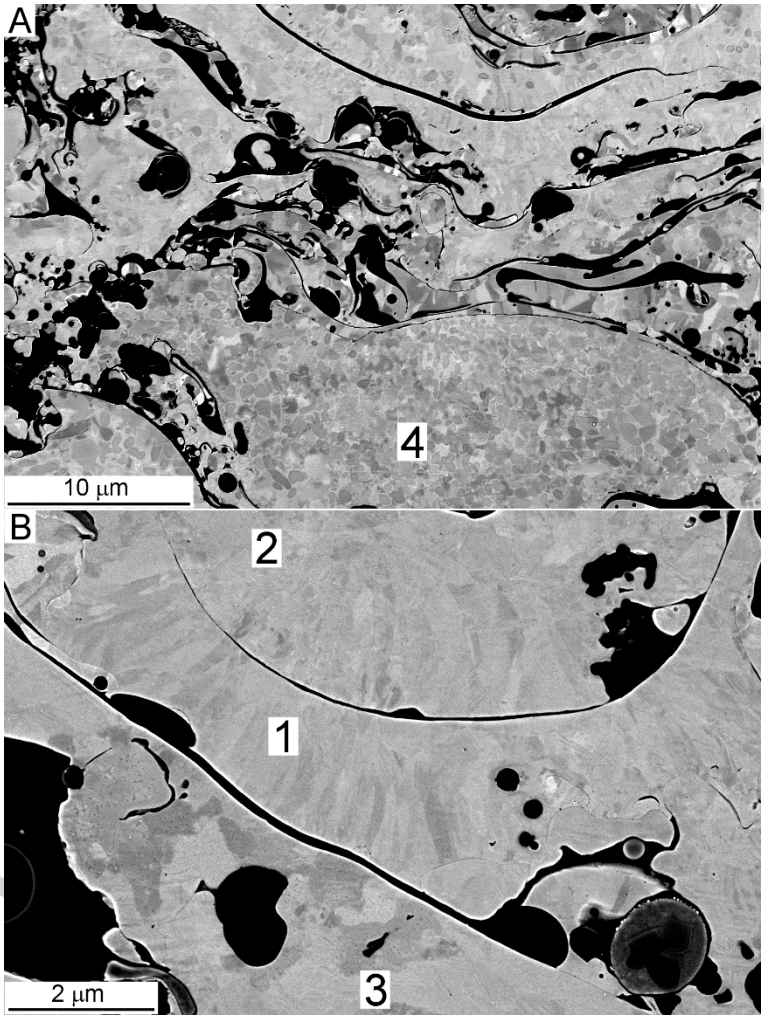

Figure 4. Detailed backscattered electron FEG-SEM micrographs showing various crystalline grain morphologies along the cross-section of the NiCrAlY + 6 wt.% Al_2O_3 sample.
Label 1 = NiCrAlY splat with columnar grains; 2 = NiCrAlY splat with equiaxed grains; 3 = NiCrAlY splat with large equiaxed grains; 4 = partly unmelted region with cellular grains.

The channelling contrast in backscatter electron images acquired at low voltages highlights a certain variety in the crystalline grain texture within the NiCrAlY lamellae (Fig. 4), probably reflecting the

different cooling rates of distinct particles. Thin, well-flattened splats (Fig. 4B, label 1) exhibit fine columnar crystals, a few hundreds of nanometres wide, extending across most or all of the thickness. Less flattened splats contain equiaxed crystals, because homogeneous nuclei inside the melt have the time to develop into crystals before heterogeneously nucleated grains at the bottom surface can grow across the entire splat (Fig. 4B, label 2). In other cases, crystals are coarser and somewhat bigger, up to 1 µm (Fig. 4B: label 3), suggesting a lower cooling rate and a possible onset of in-flight re-solidification.

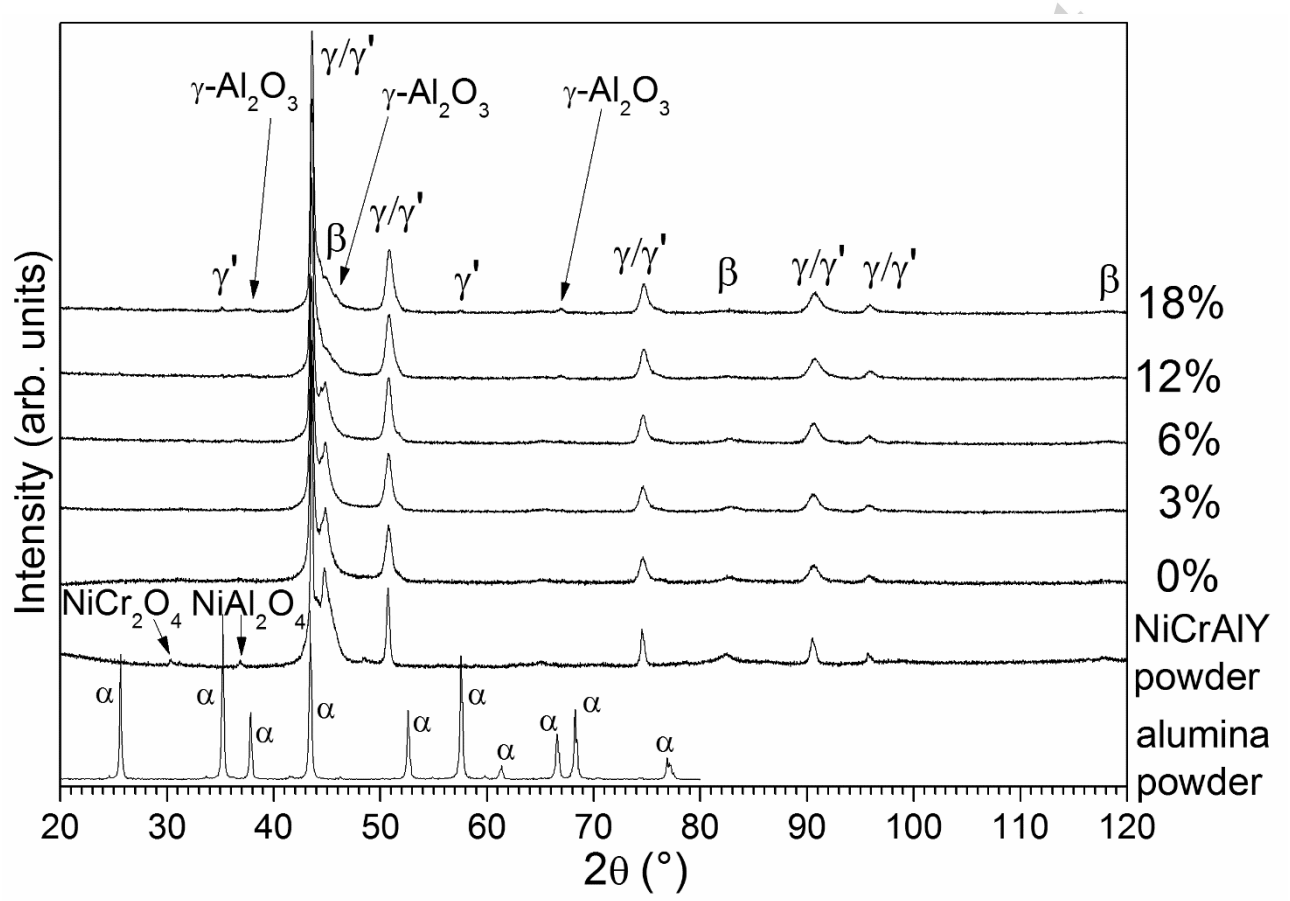

Figure 5. XRD patterns of the NiCrAlY and Al_2O_3 feedstock powders, and of all as-deposited coatings.
Legend: γ = γ-Ni (JCPDF 4-850) phase; γ′ = γ′-Ni_3Al (JCPDF 9-97); β = β-NiAl (JCPDF 44-1188); α = α-Al_2O_3 (JCPDF 46-1212); γ-Al_2O_3 (JCPDF 10-425); $NiAl_2O_4$ (JCPDF 10-0339); $NiCr_2O_4$ (JCPDF 1-75-198).

Comparison to the XRD patterns clearly suggests that all of these columnar and equiaxed crystals consist of a γ-Ni or γ′-Ni_3Al matrix, which is indeed the main phase within the coatings (Fig. 5).

The γ/γ′ peaks are significantly shifted towards lower 2θ values compared to the theoretical positions according either to JCPDF 4-850 or to JCPDF 9-97 (respectively), which indicates super-saturation with respect to solute atoms having larger atomic radii (such as Al). The formation of a super-saturated solid solution, previously observed in the literature for various plasma-sprayed MCrAlY-type alloys [30,38], is probably a consequence of the rapid cooling that is experienced by molten particles both during the gas-atomisation process and during plasma spray deposition, as described previously. Accordingly, the weak intensity of the β-NiAl peaks in the patterns of Fig. 5 indicates a lower amount of this phase than it would be expected in thermodynamic equilibrium conditions. This is particularly true for the coating samples containing the highest amount of Al_2O_3 reinforcement. In that case, more extensive melting of the NiCrAlY feedstock is favoured by the lower feed rates employed to deposit the coatings with the highest Al_2O_3 content (Table II), and/or by the increase in the temperature and thermal conductivity of the gas jet caused by the burning of vaporised ethanol, as shown e.g. in [36].

Diffraction peaks related to the Al_2O_3 phase are barely recognisable in the coatings. The main peak of α-Al_2O_3 unfortunately coincides with that of the γ/γ′ phase, but all of its other peaks are not identifiable (Fig. 5). Peaks of γ-Al_2O_3, on the other hand, emerge above the background due to the NiCrAlY matrix only in the sample containing 18 wt.% reinforcement (Fig. 5). This probably depends, on the one hand, on the low crystallinity of rapidly solidified Al_2O_3 (which turns from the thermodynamically stable α-phase into γ- and glassy-phases after thermal spraying [39,40]) and, on the other hand, to a matrix effect due to the fact that Al_2O_3 particles are surrounded by the Ni-based alloy.

The β-NiAl phase is probably recognisable in the core-shell structure of the cellular grains in the feedstock powder (Fig. 6A), a structure which is retained (Fig. 6B) in the largest and less flattened splats (such as the one seen in Fig. 4A, label 4), originating from unmolten particles. Segregation between a darker, Al-rich core and a brighter, Cr-rich boundary indeed exists within the cellular grains (Fig. 6), which is probably a result of the somewhat slower cooling during gas atomising,

compared to plasma spray conditions. Due to the very low beam energy (3 keV) needed to have sufficiently small X-ray generation volume, the yttrium peak could not be discerned; hence, its partition between the two regions could not be obtained, although the brighter rim contrast may suggest a higher concentration of Y as well.

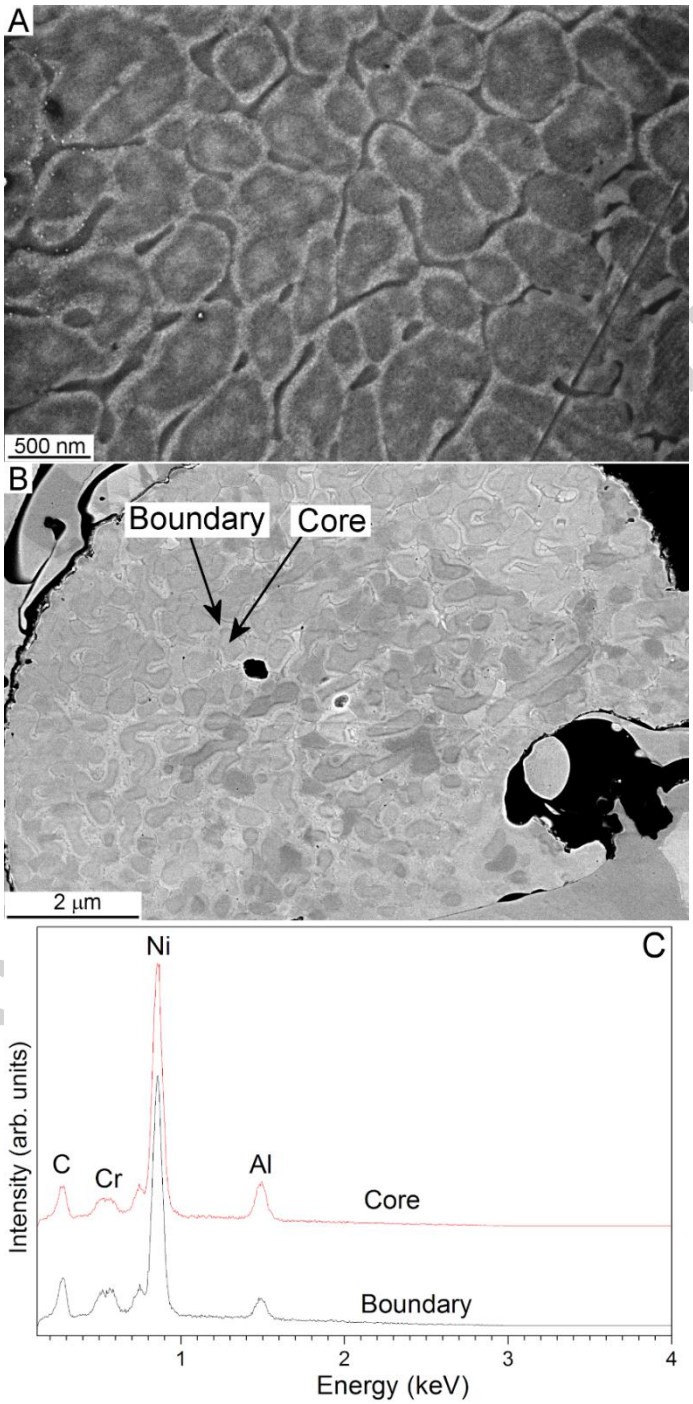

Figure 6. Detailed backscattered electron FEG-SEM micrographs of the feedstock powder (A) and of an unmelted particle in the NiCrAlY + 6 wt.% Al_2O_3 sample (B), and EDX spectra (C) acquired on the core and boundary of the cellular grains marked in panel B.

Interestingly, minor peaks of $NiAl_2O_4$ and $NiCr_2O_4$ are also seen in the pattern of the NiCrAlY powder (Fig. 5), suggesting the presence of a thin oxide shell surrounding the particles.

3.2 Microstructural and phase evolution after high-temperature exposure

After isothermal holding at 400 °C for the duration of the wear test (Section 2.2), the microstructure, oxide distribution and porosity of the samples are not perceivably altered compared to the as-deposited coatings (Fig. 7A: compare to Fig. 2). The intra-lamellar crystalline texture (Fig. 7B) is also the same as that seen in Fig. 4; namely, no recrystallization and no perceivable interlamellar boundary diffusion therefore took place. Accordingly, the XRD patterns do not change significantly (Fig. 8).

The overall microstructure remains unaltered (Fig. 7C) after holding at 700 °C as well, as this temperature is not sufficient to cause, for instance, long-range diffusion between the coating and the substrate. At the micrometre scale, however, the NiCrAlY matrix re-crystallised extensively, developing larger amounts of β-NiAl (Fig. 8) in the form of sub-micrometric precipitates of various sizes (Fig. 7D-F), which stand proud of the surrounding matrix after polishing because of their higher hardness [41]. The matrix itself is re-arranged into regular polygonal crystals (Fig. 7D-F) and its diffraction pattern, now comprising low-intensity peaks as well, can be more confidently indexed to the γ′-Ni_3Al phase. These peaks are narrower than in as-deposited condition, signifying a substantial reduction in lattice defects after re-crystallisation, and are shifted towards higher 2θ values, as seen in the detail of Fig. 8B, indicating a decrease in lattice spacing because the excess solute atoms left the matrix as the β-phase precipitated.

The size of the β-phase varies locally, sometimes entering a truly nanometre range (e.g. see circled areas in Figs. 7D,E), probably on account of small fluctuations in the local chemical composition and/or in the crystalline nature of the original material (which may also depend from the oxidation of the NiCrAlY alloy during deposition as described in Section 3.1). In any case, it is much finer

than the usual β-phase seen in NiCoCrAlY-type alloys exposed to higher temperatures in gas turbine blade applications [30–33,38].

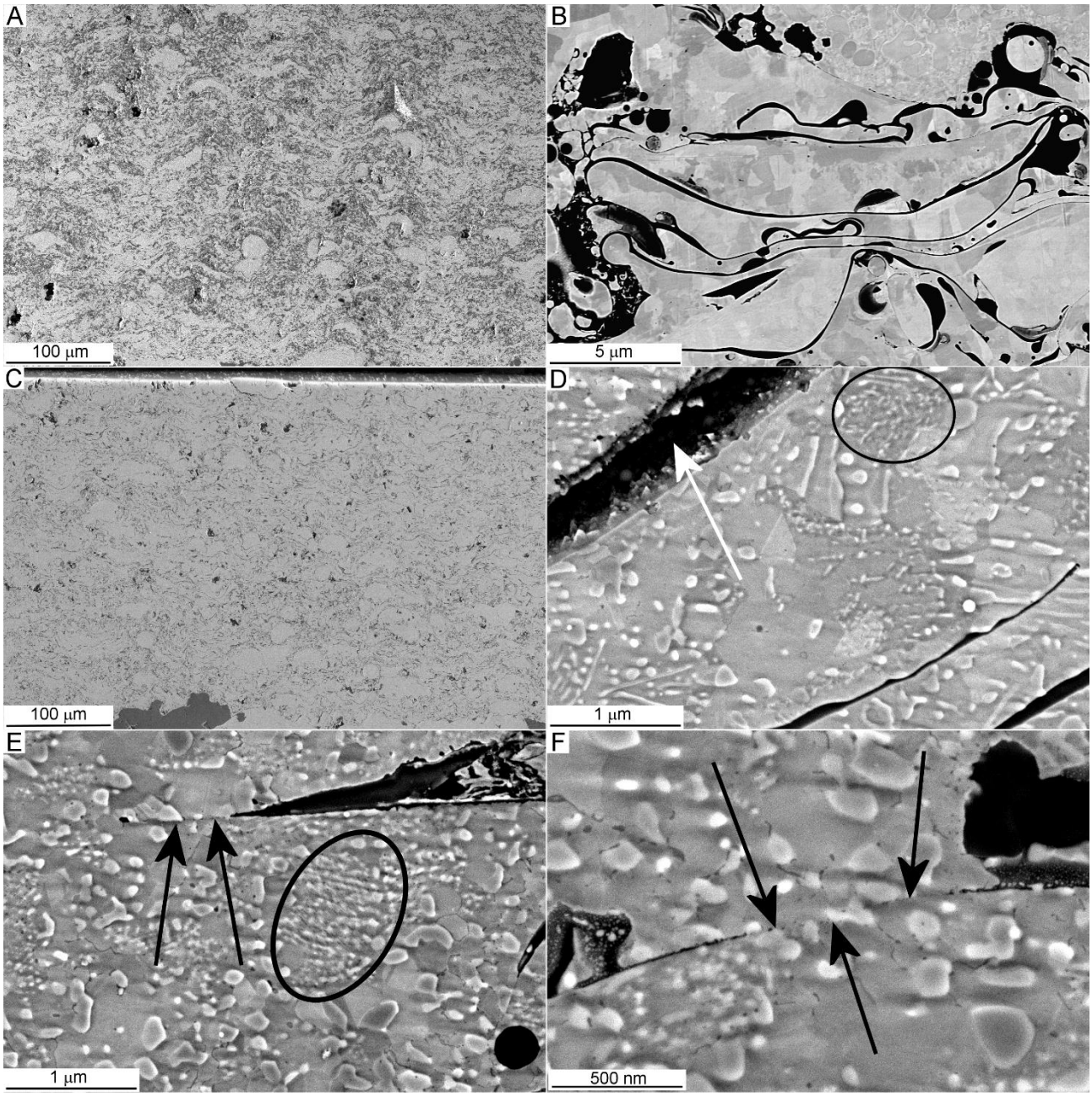

Figure 7. FEG-SEM micrographs of the cross-sections of the coatings after isothermal holding at 400 °C (A: secondary electrons overview of the NiCrAlY + 18wt.% Al_2O_3 sample; B: backscattered electron detail of the NiCrAlY + 3wt.% Al_2O_3 sample) and at 700 °C (C: secondary electrons overview of the NiCrAlY sample; D-F: backscattered electron details of the NiCrAlY + 6wt.% Al_2O_3 sample) during the wear test.

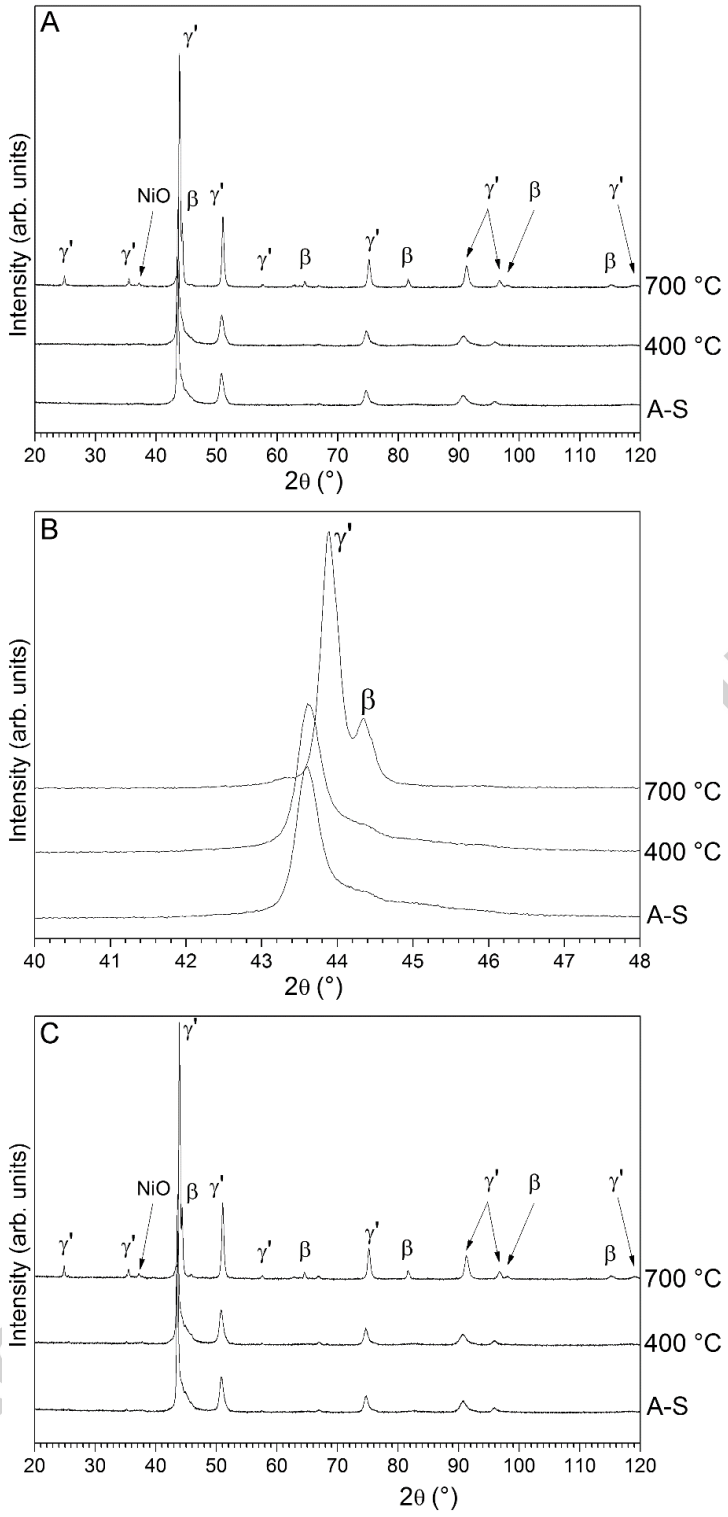

Figure 8. XRD patterns of the coatings containing 12 wt.% (A: overview, B: detail of the main peaks area) and 18 wt.% (C) Al_2O_3 after isothermal holding at 400 °C and 700 °C during the wear tests, compared to the patterns in as-deposited condition (labelled "A-S" in the graphs).

Although large-scale diffusion did not take place, small-scale diffusion along the boundaries between the NiCrAlY lamellae did occur, with local re-organisation of thin interlamellar oxides as

seen in Figs. 7E,F (see arrows). This may help promoting better interlamellar cohesion within the metal matrix, although this process could not take place when the interlamellar oxide layer was too thick or when relatively wide interlamellar voids existed (Fig. 7D, arrow).

It is important to remind that these observations refer to the microstructure seen after cooling down to room temperature, whilst the wear test occurred at high temperature. Nonetheless, it is clear that the re-crystallisation of the NiCrAlY matrix, the β-phase precipitation, and the partial healing of some of its interlamellar boundaries have an effect on the mechanical properties and on the wear behaviour, which will be discussed in detail in the forthcoming Sections 3.3 and 3.4 respectively.

3.3 Micromechanical properties

The as-deposited samples and those tested at 400 °C exhibit analogous hardness values (consistent with the absence of microstructural alterations, Section 3.2), which tend to increase with the amount of Al_2O_3 up to 12 wt.% (Fig. 9A). The increase, however, is not very remarkable, probably because of a somewhat limited cohesion of the Al_2O_3 particles with the surrounding NiCrAlY lamellae. Whilst some of the indentation marks (e.g. see Figs. 2C,E) do not cause clear failure of the material (though the possibility of sub-surface cracking, as shown in [42] for a different type of plasma-sprayed coating, cannot be ruled out), others do exhibit cracking and material uplifting (Fig. 9C, see arrow).

Even though indentation marks with extensive cracking and/or with ill-shaped load-displacement curves were discarded from the analysis (see Section 2.3), interface sliding between the NiCrAlY matrix and the Al_2O_3 particles is probably occurring in all cases. This limits the load transfer between the two phases and reduces the increase in hardness below the level that would be expected based e.g. on a simple rule-of-mixture approach. Further increase of the Al_2O_3 content up to 18 wt.% even causes hardness to drop down again, probably because of the excess amount of defects generated by clustering of Al_2O_3 particles (Section 3.1 and Figs. 2E, 3B and 7A).

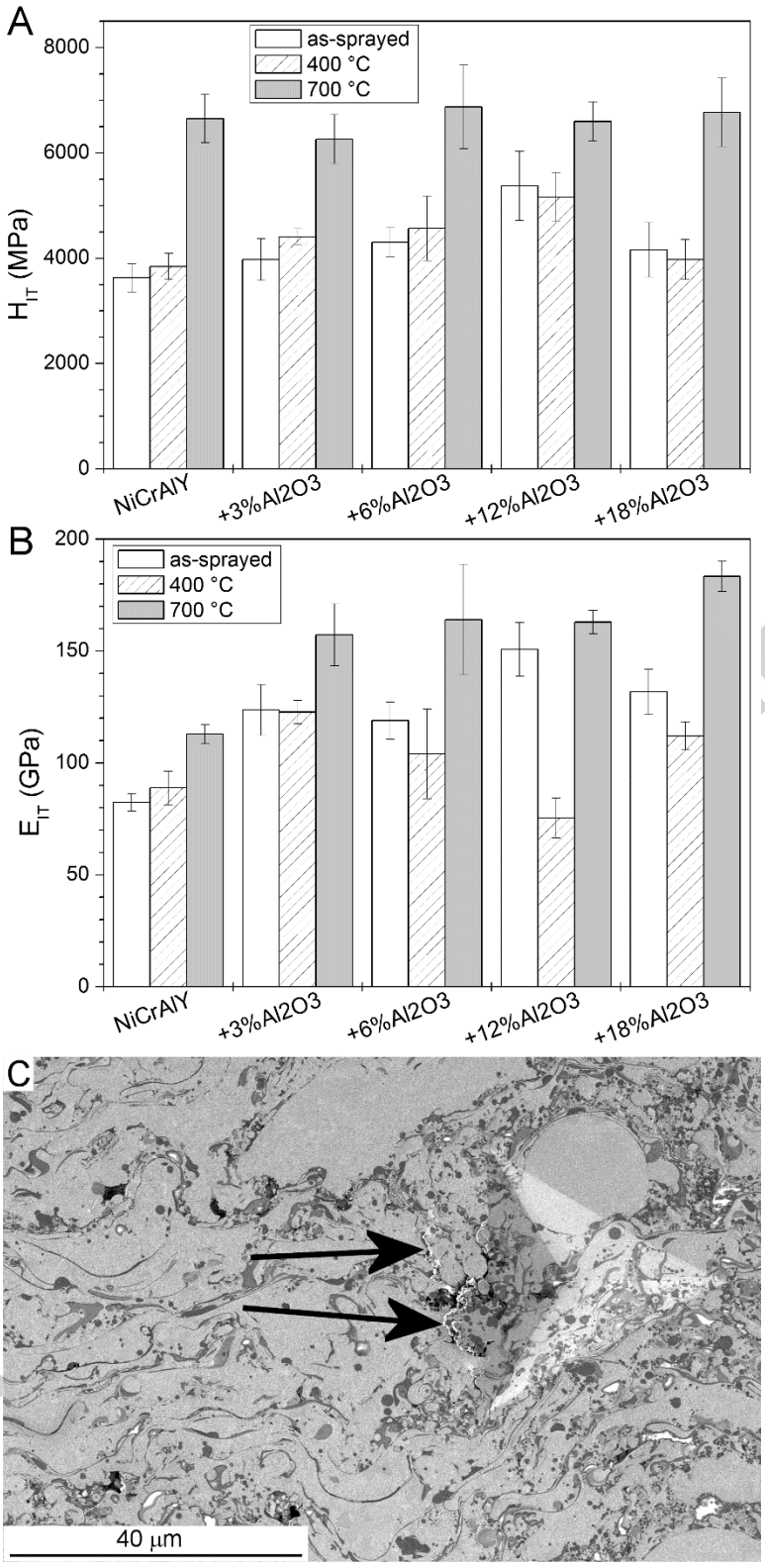

Figure 9. Hardness (A) and elastic modulus (B) values measured by depth-sensing Berkovich micro-indentation on all samples before and after isothermal holding at 400 °C and 700 °C during the wear tests, and (C) FEG-SEM micrograph of a microindentation with evidence of local failure in a defective area (arrows).

After holding at 700 °C, by contrast, hardness values increase significantly and become substantially insensitive of the Al_2O_3 content. Hardness is enhanced because of the improvements in both intra-lamellar strength (thanks to the precipitation of the hard [41], finely dispersed β-phase) and interlamellar cohesion (thanks to the healing of interlamellar boundaries), as discussed in Section 3.2. Those effects definitely prevail over that of the Al_2O_3 reinforcement, as the cohesion of the latter with the surrounding matrix remains limited: diffusion is not expected to affect Al_2O_3 at 700 °C.

Analogous considerations on interlamellar healing and intra-lamellar hardening were given in [43] in relation to a similar increase in the hardness of atmospheric plasma-sprayed NiCoCrAlY after exposure at 1100 °C. The hardness of the pure NiCrAlY coating (≈3500 MPa, Fig. 9A) is indeed consistent with the values reported in the literature for atmospheric plasma-sprayed NiCoCrAlYs [43,44].

Trends in the values of elastic modulus (Fig. 9B) are comparatively less obvious, although the reliability of the measurement is testified by the consistency of the value measured on the as-deposited pure NiCrAlY (≈80 GPa) with literature data for similar coatings [45,46]. Nonetheless, it is quite clear that the elastic modulus of the as-deposited coatings also tends to increase with the amount of Al_2O_3 up to 12 wt.%, and that it increases after the sample is held at 700 °C, in accordance with the previous considerations on healing of the lamellar boundaries between NiCrAlY particles.

3.4 Sliding wear behaviour

3.4.1 General considerations

Sample wear rates (Fig. 10A) and friction coefficients (Fig. 10B) show some remarkable trends:

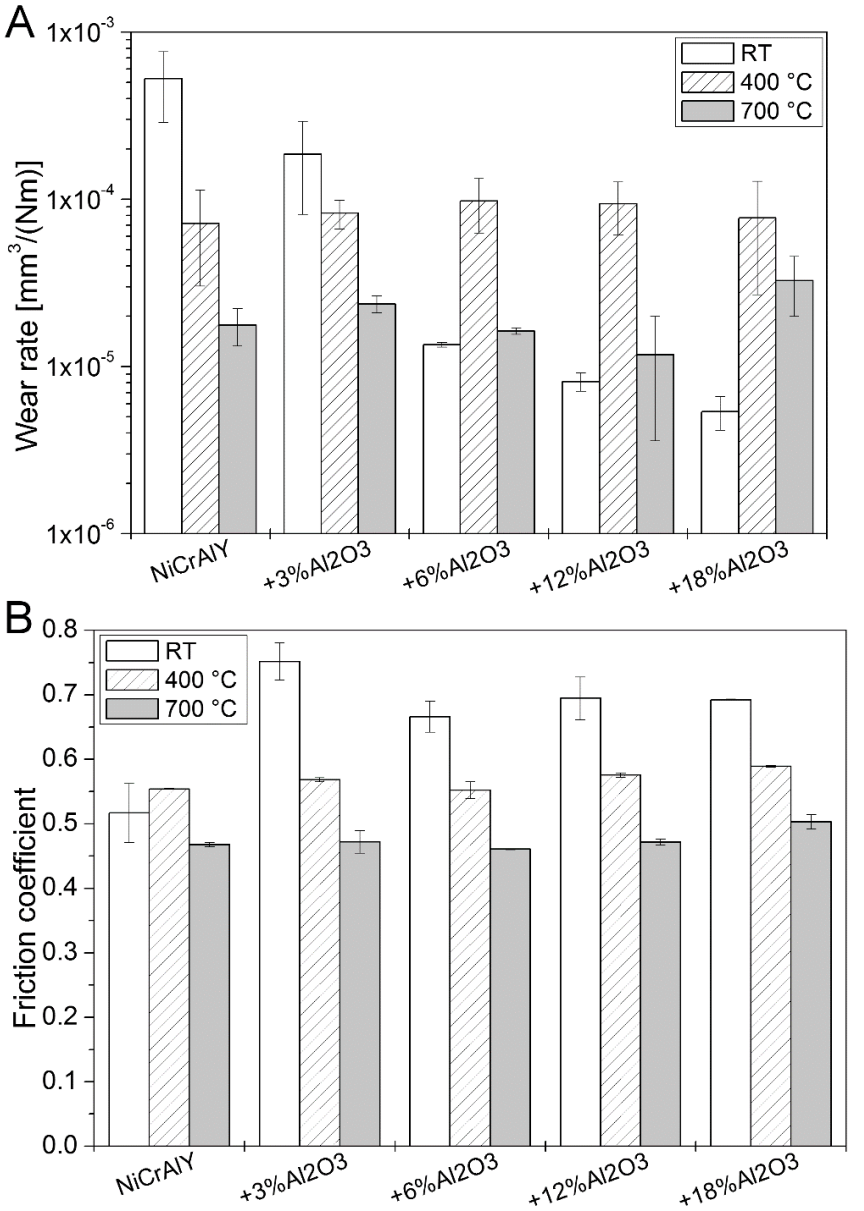

Figure 10. Wear rates (A) and friction coefficients (B) measured by ball-on-disk sliding wear tests at room temperature, 400 °C and 700 °C (average ± standard deviation).

1) The wear rate of the pure NiCrAlY coating at room temperature is $\approx 5*10^{-4}$ mm^3/(Nm). As a term of comparison, this value is more than one order of magnitude higher than that of thermally sprayed Fe-Cr-B and Ni-Cr-B-Si coatings, tested under identical conditions by the authors in previous works ($\approx 1 - 5 *10^{-5}$ mm^3/(Nm)) [47–49].

Addition of up to 6 wt.% of Al_2O_3 causes the wear rate at room temperature to decrease down to $\approx 1*10^{-5}$ mm^3/(Nm). For increasingly high amounts of Al_2O_3, wear rates tend towards a plateau of

≈6-10^{-6} mm^3/(Nm), i.e. lower than those of the previously mentioned, unreinforced Fe-Cr-B and Ni-Cr-B-Si coatings.

The steady-state friction coefficient, on the other hand, is lower (≈0.5) for the pure NiCrAlY coating than for the composite coatings (≈0.7).

2) At 400 °C and 700 °C, wear rates and friction coefficients are independent of the amount of Al_2O_3. Specifically, the values of wear rate and friction coefficient are lower at 700 °C (≈2*10^{-5} mm^3/(Nm) and ≈0.45, respectively) than at 400 °C (≈8*10^{-5} mm^3/(Nm) and ≈0.55, respectively). This also means that, whilst the wear loss of the unreinforced NiCrAlY coating decreases continuously from room temperature to 400 °C and 700 °C, the wear losses of the composite coatings with 6 – 18 wt.% Al_2O_3 are lower at room temperature than at 400 °C.

Compared to the mentioned Fe-Cr-B and Ni-Cr-B-Si references [47–49], the performance of the NiCrAlY samples is slightly better at 400 °C (where the reference materials exhibit wear rates of (≈1*10^{-4} mm^3/(Nm)) and significantly better at 700 °C (where the reference wear rates are >3*10^{-4} mm^3/(Nm)). The wear rates of the present samples are of the same order of magnitude as those of thermally sprayed or cladded MCrAlY-type coatings (with M = Ni and/or Co) tested by other authors under similar (though not identical) ball-on-disk conditions against ceramic counterparts [11,24,25,50].

3.4.2 Wear mechanisms at room temperature

A more detailed analysis of wear mechanisms indicates that, at room temperature, the pure NiCrAlY coating suffers severe adhesive/delaminative wear (Fig. 11). The coating surface is plastically deformed in the direction of sliding, as the ball surface adheres to the softer NiCrAlY and drags it along its sliding motion. Repeated adhesion and shear deformation result either in the extrusion of lips of materials, the tips of which are progressively fragmented (Fig. 11, label 1: compare the similarity of this lip with the adhesive wear morphology shown in [51]), or in the direct delamination of some portions of material (Fig. 11, label 2). The latter is favoured by the limited

interlamellar cohesion of the as-deposited coatings (in accordance with their lower hardness and modulus, Section 3.3) and by the possible presence of brittle interlamellar oxide inclusions (Section 3.1 and Fig. 3D).

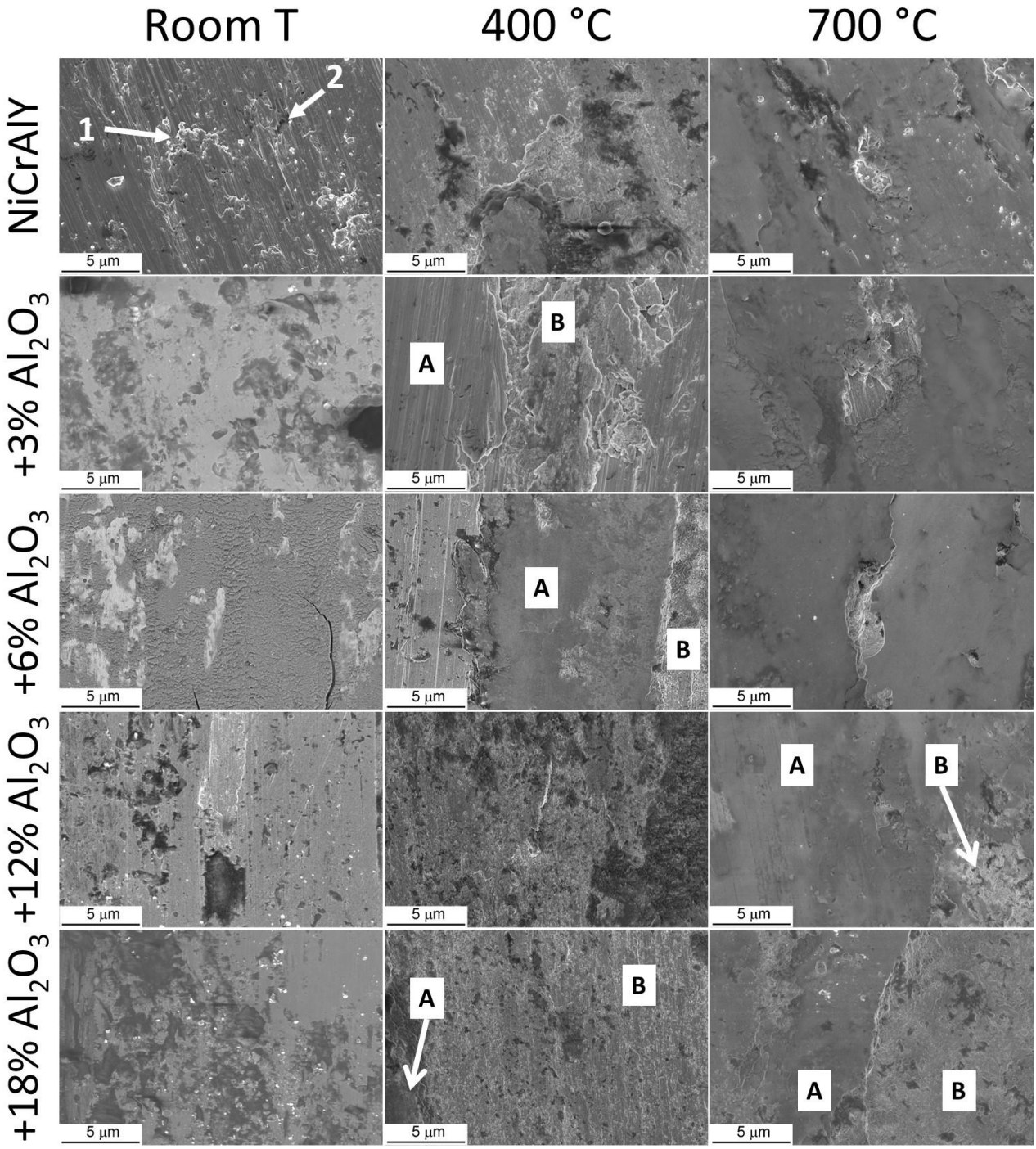

Figure 11. FEG-SEM micrographs of the top surfaces of the wear scars on the coated samples.

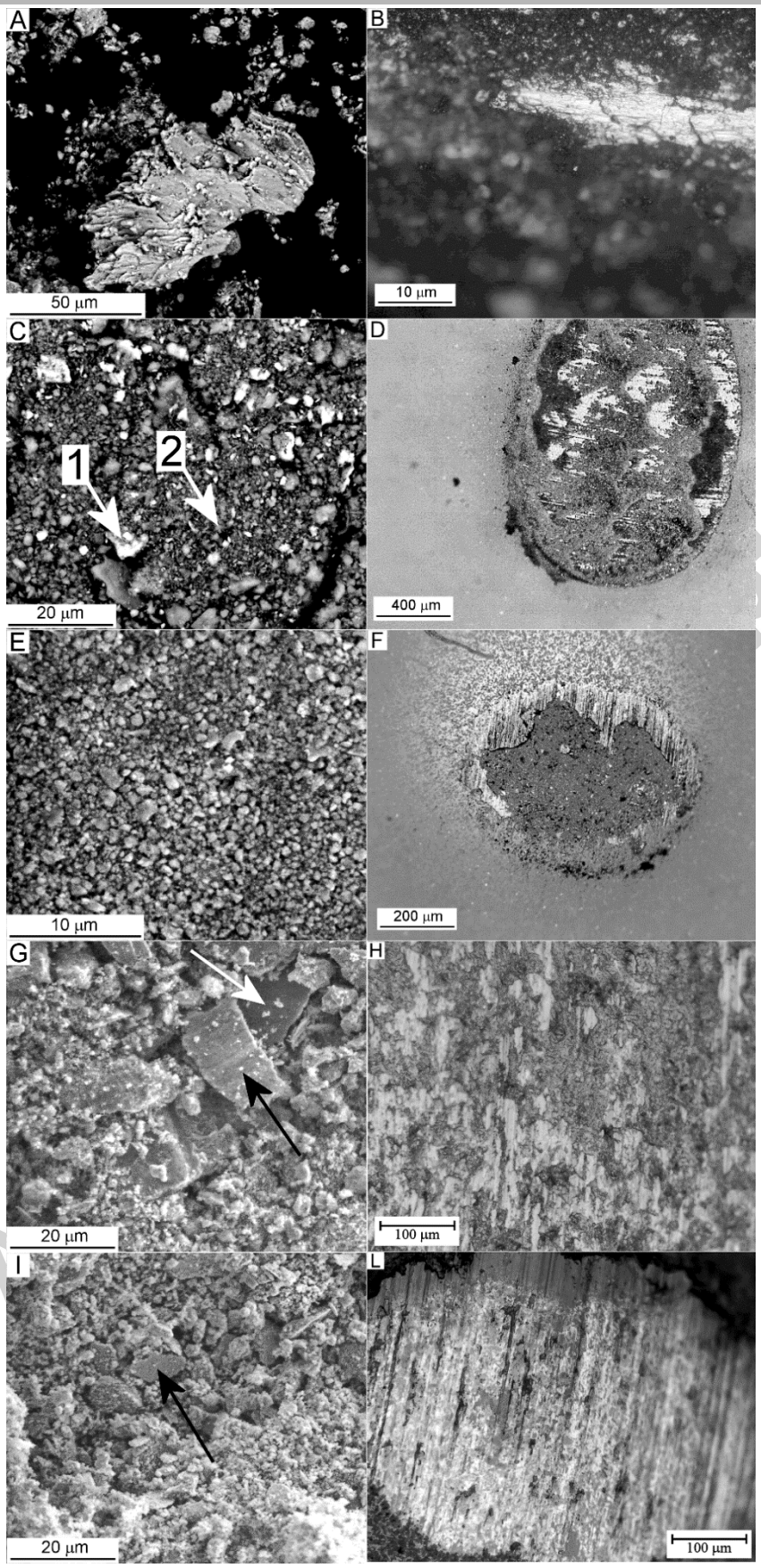

Figure 12. SEM micrographs of the loose wear debris and optical micrographs of wear scars on the counterbodies: pure NiCrAlY, room T (A,B); NiCrAlY+6%Al_2O_3, room T (C,D); NiCrAlY+12%Al_2O_3, room T (E,F); NiCrAlY+12%Al_2O_3, 400 °C (G,H); NiCrAlY+12%Al_2O_3, 700 °C (I,L).

Similar adhesive/delaminative wear mechanisms, involving either the direct removal of lamellae or their plastic extrusion (leading to the detachment of fragments from their uplifted tips), have accordingly been observed in thermal spray metallic coatings subjected to sliding wear in operating environments, such as cylinder liners in internal combustion engines [52] or radial hydraulic motors [53]). This testifies to the representativeness of the present test conditions, which manage to reproduce actual wear mechanisms, and to the significance of the results.

The loose debris collected outside the wear scar after the test accordingly contains large pieces of metallic material (Fig. 12A), which were plastically deformed and elongated into a platelet morphology typical of adhesive wear [54]. A layer of transferred metal was also built up onto the surface of the counterpart (Fig. 12B), and the significant noise of the friction curve of the pure NiCrAlY coating (Fig. 13A) reflects the stick-slip phenomena associated to the continuous formation and rupture of surface junctions between the sample and the counterbody. The overall system wear, monitored (at least qualitatively) by the on-line measurement of the ball-holding arm position, increases almost linearly after an initial running-in stage (Fig. 13A). This reflects a continuous increase of the groove depth on the coating surface, as the ball experiences very limited wear loss. Gentle removal of the transfer layer by polishing with a colloidal silica suspension, indeed, reveals that the ball keeps a curved surface, without developing a flattened worn cap (Fig. 13B). This also means that measurements of ball wear loss are not possible. Any removal of the transfer layer (either by mechanical methods, as it was done in Fig. 13B, or by chemical ones) might indeed alter, albeit slightly, the underlying ceramic surface; hence, a quantitative comparison between the original and worn surface profiles would not be fully reliable and the analysis can only have qualitative meaning.

Addition of Al_2O_3 reinforcement into the coatings reduces adhesive tearing (Fig. 11). The morphology of the wear debris is accordingly very different from the previous one (Fig. 12C,E) and comprises numerous sub-micrometric, oxidised particles (label 2 in Fig. 12C), typical of tribo-

oxidation mechanisms [55–57]. Part of this debris is smeared and compacted onto the wear scar (Fig. 14A-D: arrows mark the debris layer), in accordance with the wear mechanism depicted e.g. in [55], and onto the counterbody surface (Fig. 12D,F). High magnification views (Fig. 14B,D), indeed, allow the recognition of such sub-micrometric particles within the tribo-layer, which provides discontinuous coverage of the wear scar (Fig. 11).

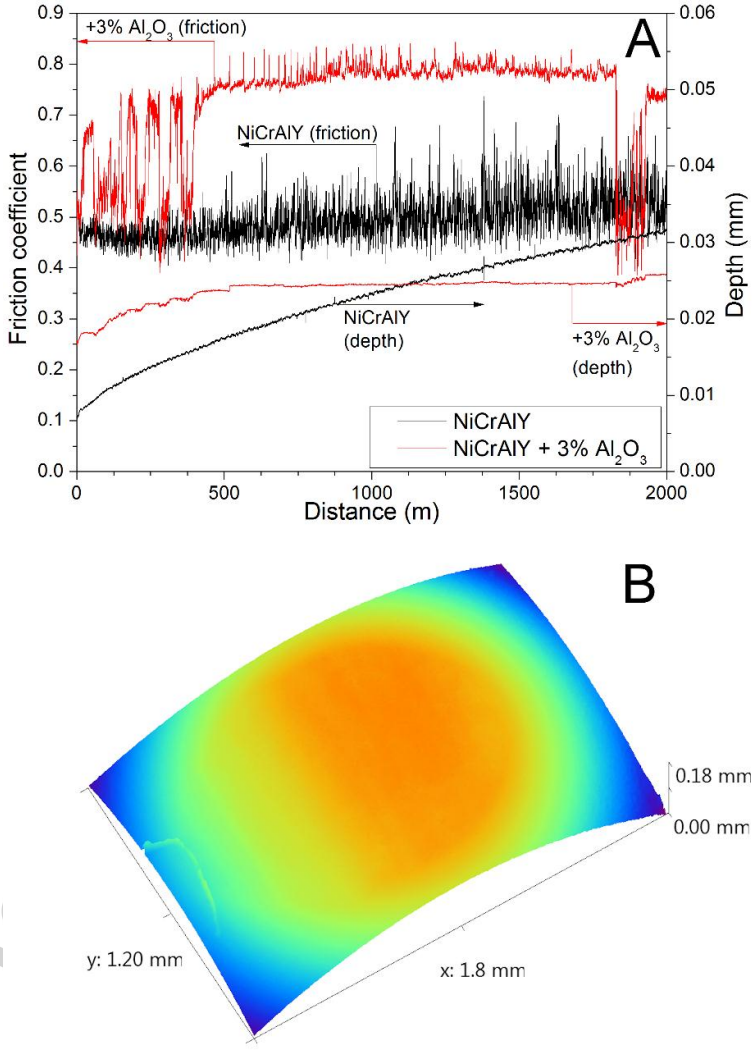

Figure 13. Evolution of the friction coefficient and of the overall wear depth recorded during room-temperature ball-on-disk wear tests on the NiCrAlY and NiCrAlY+3 Al_2O_3 samples (A) and 3D profile of the worn surface of the counterpart tested against the NiCrAlY sample at room temperature, after removal of the transfer layer (B).

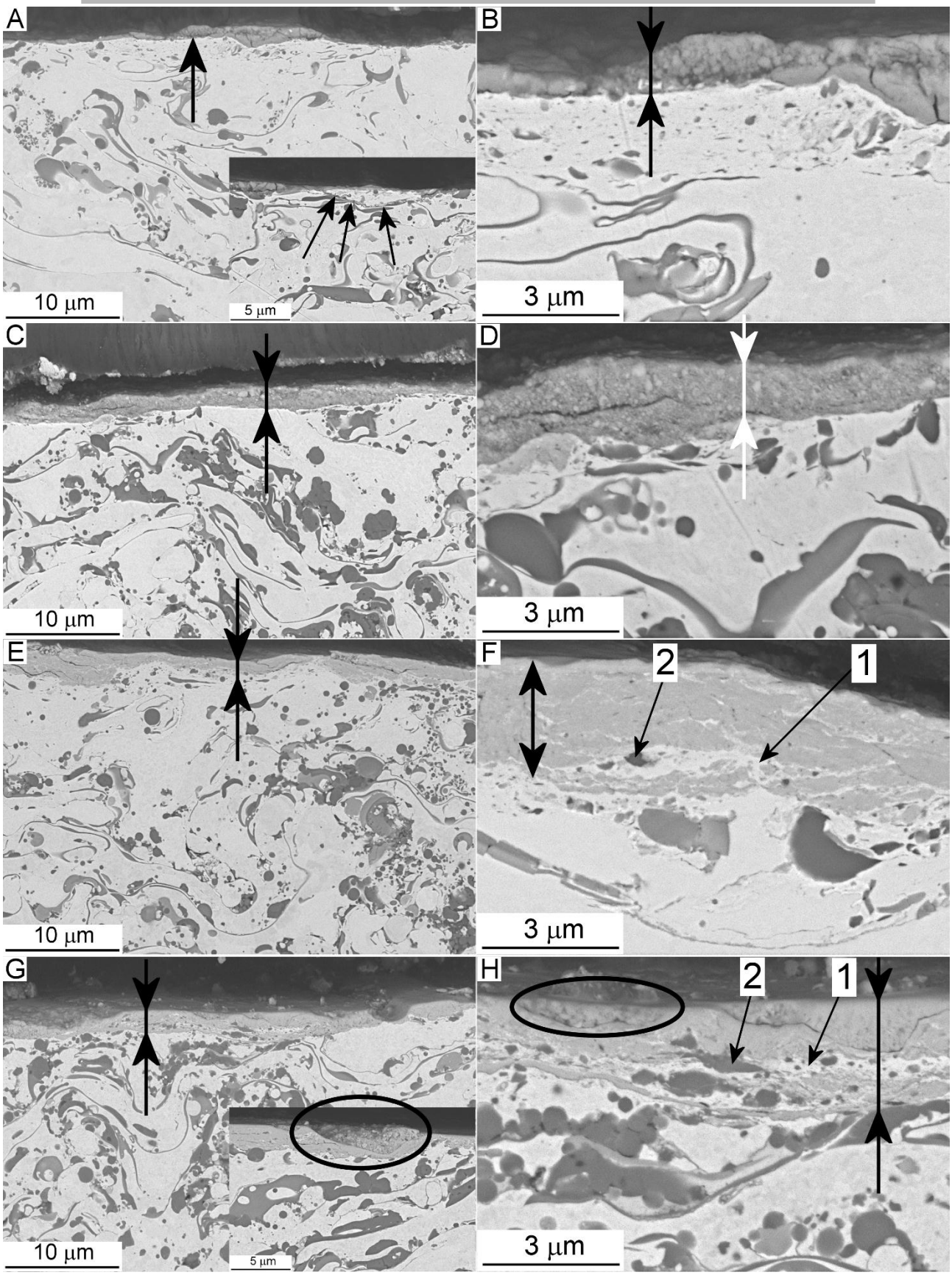

Figure 14. Cross-sectional FEG-SEM micrographs of the wear scars produced at room temperature on NiCrAlY+3%Al_2O_3 (A,B) and NiCrAlY+18%Al_2O_3 (C,D) samples, at 400 °C on NiCrAlY+3%Al_2O_3 (E,F), and at 700 °C on NiCrAlY+18%Al_2O_3 (G,H).

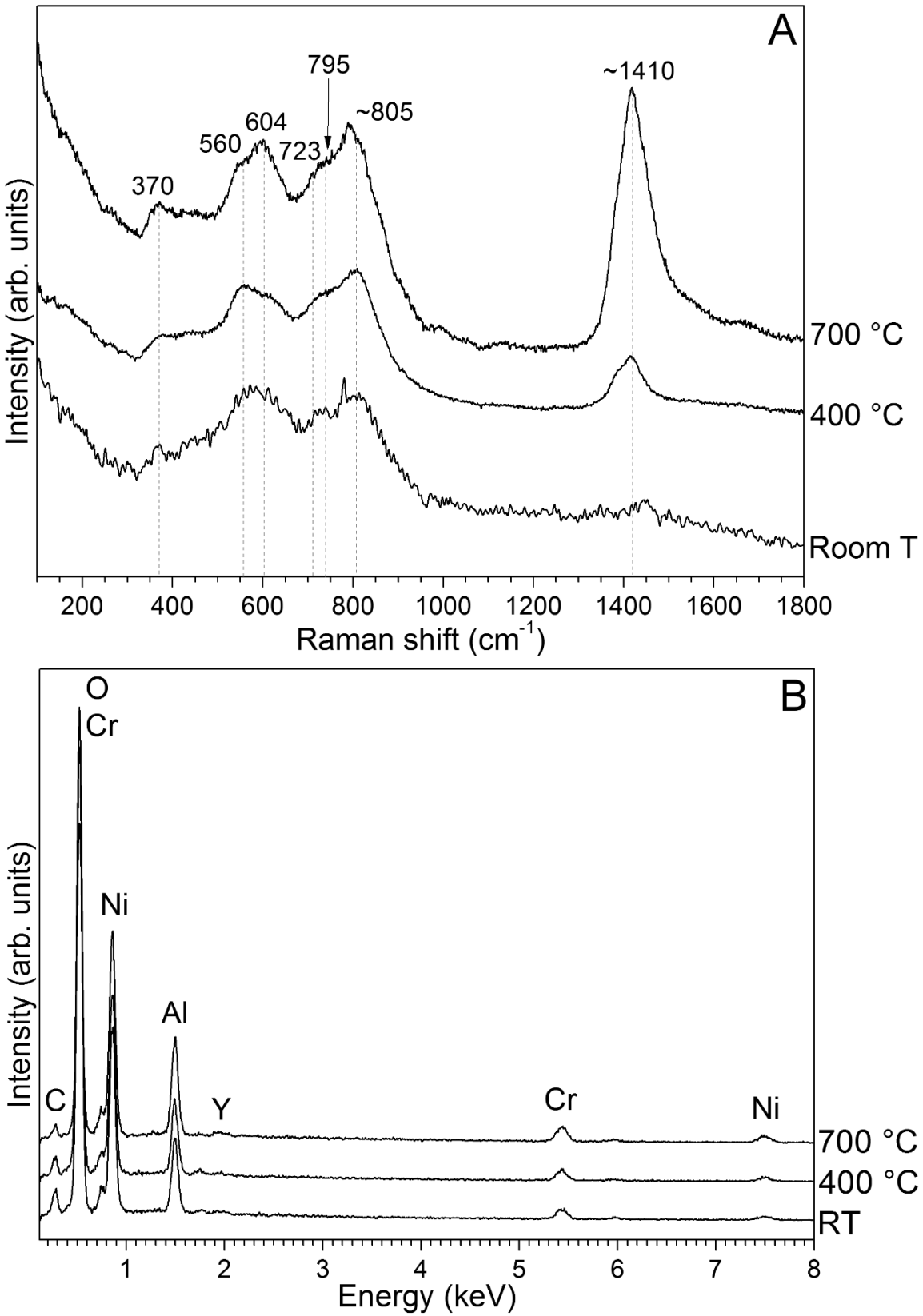

Figure 15. Representative Raman spectra (A) and EDX spectra (B) of the oxide scale formed after ball-on-disk sliding wear testing on the NiCrAlY+12%Al_2O_3 sample at the various temperatures. The main Raman peak positions are labelled in panel A.

The chemical composition of the layer (Fig. 15B) comprises all of the alloy elements and its typical Raman spectrum (Fig. 15A) presents a series of peaks at about 370, 560, 604, 723, 795 and ~805 cm^{-1}, which correspond to $NiAl_2O_4$ structure in accordance with [58]. The high intensity of the peak at ~805 cm^{-1} may also indicate the simultaneous presence of a $NiCr_2O_4$-type compound [59]. The breadth of these peaks suggests high structural disorder [60]. The smeared debris composing the tribo-layer therefore consists of comminuted metal fragments that were completely oxidised [55]. The marginal increase in hardness (Section 3.3 and Fig. 9A) cannot account for the remarkable change from adhesive wear to tribo-oxidation in the reinforced samples. Most importantly, wear keeps low in the sample containing 18 wt.% Al_2O_3 in spite of its decreased hardness (Section 3.3). The length scale of the local adhesive contacts between the coating and the counterpart (as inferable from Fig. 11) is indeed much smaller than the indentation size (Figs. 2C,E and 9C), so there is no direct relation between asperity-level contact behaviour and indentation responses.

From backscattered electron-SEM micrographs (Fig. 16A) and EDX analyses (Fig. 16B) of the wear scars, it is inferable that the Al_2O_3 particles in the composite coatings (Fig. 16A – label 1) are progressively fragmented, pulled out of the coating and smeared onto its surface. This phenomenon, which probably starts after a brief running in as previously seen in Fig. 13A, limits the occurrence of direct adhesion of the metal to the ball surface. Moreover, this provides an initial "reservoir" of very fine debris particles: according to [56,57], debris compaction into tribofilms (such as those seen in Figs. 11 and 14A-D) occurs only when its size is smaller than a critical threshold. Early development of the tribofilm is therefore promoted and, as the NiCrAlY matrix experiences some damage, the comminuted and tribo-oxidised metal fragments enter the growing tribo-layer (in accordance with the tribo-oxidation mechanisms described in [55–57,61]). A significant amount of oxides, whose intermediate greyscale-level contrast corresponds to tribo-oxidised NiCrAlY fragments, is indeed seen in Fig. 16A (EDX spectrum in Fig. 16B – label 2).

It can therefore be stated that the limited cohesion of the Al_2O_3 particles with the surrounding metal matrix (as discussed in Sections 3.1 – 3.3), which may have *a priori* appeared as a drawback, is

instead the factor that makes them so effective in changing the wear mechanism starting from an early stage.

Some adhesive/delaminative wear still occurs on the coating containing 3 wt.% Al_2O_3, as revealed by small metallic particles in the wear debris (Fig. 12C – label 1) and by bright metallic material partly covering the counterbody (Fig. 12D). Delamination is confined to the very surface of the coating. In accordance with the model given in [52], microcracks sometimes propagate along the boundary of the lamellae exposed to the outer surface (one of them is marked by arrows in the inset of Fig. 14A). Apart from that, however, no cracking occurs across the coating thickness (Fig. 14A,B).

Correspondingly, at the early stages of the test on this sample, there are sharp, abrupt transitions between lower-friction/higher-wear periods, when direct contact between the coating surface and the counterbody probably occurs, and higher-friction/lower-wear periods, when the tribofilm is interposed (Fig. 13A). Such regimes are quite typical of the low-temperature sliding wear behaviour of those Ni- and Co-based metal alloys that are capable of developing oxidised debris layers [50,55,56]. As the test progresses, the low-wear conditions become more stable (Fig. 13A), probably because of the continuous addition of smeared debris particles. The low-wear regime can however be intermittently broken down, as seen towards the end of the testing period. Various microcracks in this layer of compacted debris particles are indeed easily identifiable in Fig. 14B. Delamination of the tribofilm, with the corresponding transition to a high-wear regime, becomes less frequent with increasing Al_2O_3 content. The tribofilm indeed becomes more continuous (compare Fig. 14C to Fig. 14A), though it is not free of defects and microcracks (Fig. 14C,D). A layer of smeared oxides (Fig. 12F) also covers the ball surface and the debris consists solely of very fine, rounded oxide particles (Fig. 12E).

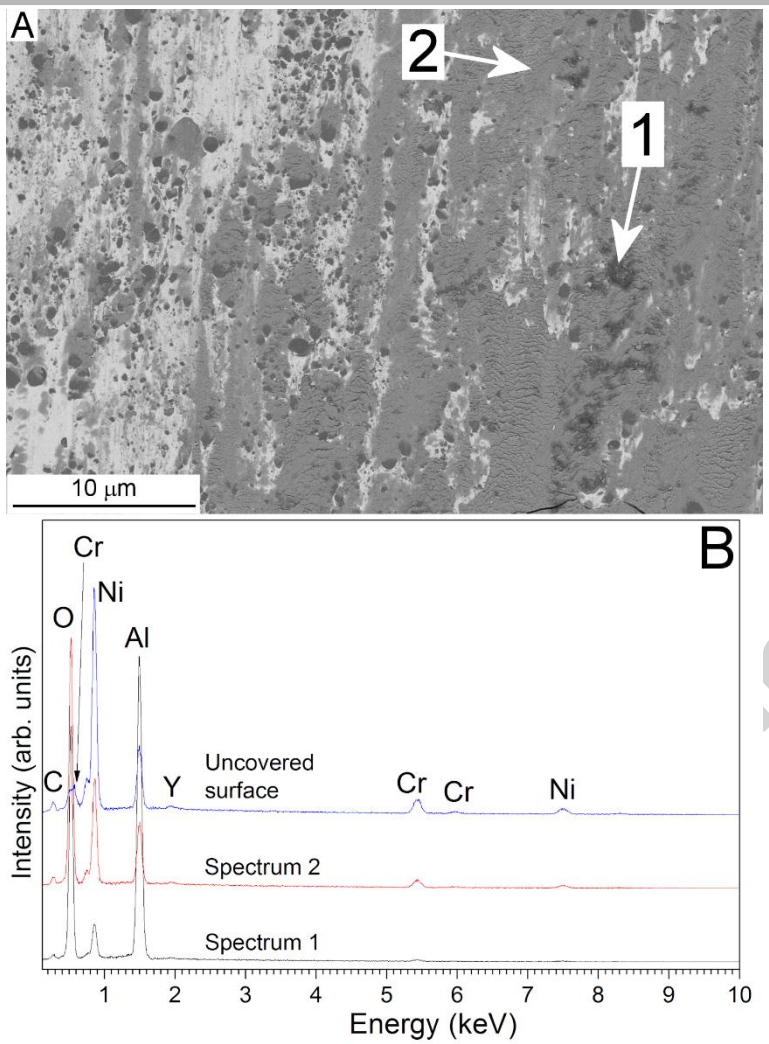

Figure 16. (A) Backscattered electrons FEG-SEM micrograph of the wear scar produced by room-temperature ball-on-disk testing of the sample containing 12 wt.% Al_2O_3, and (B) corresponding EDX spectra acquired on oxidised areas 1 and 2 and on bright, uncovered metal areas.

From these results, it also appears that the interposition of the tribofilm does not reduce friction, compared to a condition of direct adhesion between the coating and the counterbody. The oxidised debris particles covering the two mating surfaces interact strongly: the normal and shear stresses needed to break the adhesive junction between fine particles indeed grow with the reciprocal of the particles' diameter according to [56]. High tangential forces are developed, which even result in dragging of the tribofilm into an undulated, "wavy" morphology, as seen e.g. in Fig. 11 on the NiCrAlY+6%Al_2O_3 sample.

3.4.3 Wear mechanisms at high temperatures

At 400 °C and 700 °C, the performance levelling is related to the onset of an identical tribo-oxidation wear mechanism on all coatings. All wear scars are indeed quite uniformly covered by an oxide tribo-layer (Fig. 11 and Fig. 14E-H) comprising smooth areas (label "A" in Fig. 11) and rougher areas (label "B" in Fig. 11). Such type of tribo-layers are often termed "glaze" in the pertinent literature [11,24,25,50,55,56].

The cross-sections of the "glaze" layers reveal a dense oxide scale, a few micrometres thick (Fig. 14F,H), which probably corresponds to the smooth areas, and which differs substantially from the compacted debris layer found at room temperature (Fig. 14B,D). The scale is indeed fully dense, without recognisable particles, and, particularly in its lower portion, it encompasses bright, non-oxidised remains of the NiCrAlY alloy (Fig. 14F,H: label 1) and non-fragmented Al_2O_3 reinforcement (Fig. 14F,H: label 2). These observations indicate that the scale grows by direct tribo-oxidation of the NiCrAlY metal, a process which has indeed been documented various times in the literature [62,63].

Wear proceeds by the periodic cracking, spallation and regeneration of the "glaze" film, which indeed contains visible microcracks (Fig. 14E-H). Accordingly, the wear debris (Fig. 13G,I) contains larger, platelet-like oxidised particles (marked by arrows), resulting from local spallation of the "glaze", in addition to finer, sub-micrometric particles, originated by further comminution of the larger particles. The fine particles can be smeared and compacted again onto the wear scar (similar to the situation at room temperature), filling in the areas where the "glaze" was delaminated, as seen in the circled areas of Fig. 14G,H. This gives rise to the rougher tribofilm regions (label "B" in Fig. 11).

The "glaze" film is much thicker than the oxide layer spontaneously developed outside the wear scar. At 400 °C, the latter consists of nanometric oxide protrusions (Fig. 17A – label 1); at 700 °C, it turns into a fine-grained layer (Fig. 17C – label 2) with some thicker, faceted clusters (Fig. 17B,C

– label 3). In either case, the oxidised layer is so thin, that it is undiscernible in cross-sectional views (Fig. 17E,F). For this reason, its chemical composition could not be obtained by EDX, micro-Raman spectroscopy or XRD (even under grazing incidence conditions). EDX spectra acquired at very low beam energy (Fig. 17D – spectrum 1 and 2) could only confirm the presence of some oxygen onto these surfaces. Surface-sensitive analyses such as XPS should probably be employed for this purpose; however, such detailed analysis is outside the scope of this paper. By analogy with the extensive literature on MCrAlY materials [30–32,38,43,64], these oxides can be thought to consist of Al_2O_3. Only the faceted clusters could be clearly identified as NiO (Fig. 17D, spectrum 3), growing preferentially along lamellar boundaries (Fig. 17B) as these are depleted in Al and Y due to in-flight oxidation as discussed in Section 3.1. This is a typical issue with the high temperature oxidation behaviour of MCrAlY coatings deposited by atmospheric plasma spraying [30–32,64], but it is probably not that deleterious at the present temperature of 700 °C, much lower than the values of 900 – 1000 °C experienced when MCrAlYs are employed as oxidation-resistant layers on turbine blades and vanes [7].

In accordance with the literature on bulk Ni- and Co-alloys [62,65], the thickening of the scale inside the wear scar is ascribed to two concurrent mechanisms:

(i) The development of high flash temperatures in the contact point, accelerating the oxidation kinetics. Some researchers argue that flash temperatures are also associated with the exo-emission of electrons (“triboemission”) [66,67], due to thermionic effects and to the accumulated strain energy becoming larger than the bond energy [68]. In the surroundings of the extremely small contact area, the triboemission reportedly generates a triboplasma containing active species (radical and ions) which accelerate all tribochemical reactions. This explains why, in spite of their extremely short-lived existence, flash temperatures can substantially modify oxidation processes [68]. The mechanism has been described primarily in relation to tribochemical phenomena in boundary lubrication [66–68], but it may equally act in case of high-temperature tribo-oxidation.

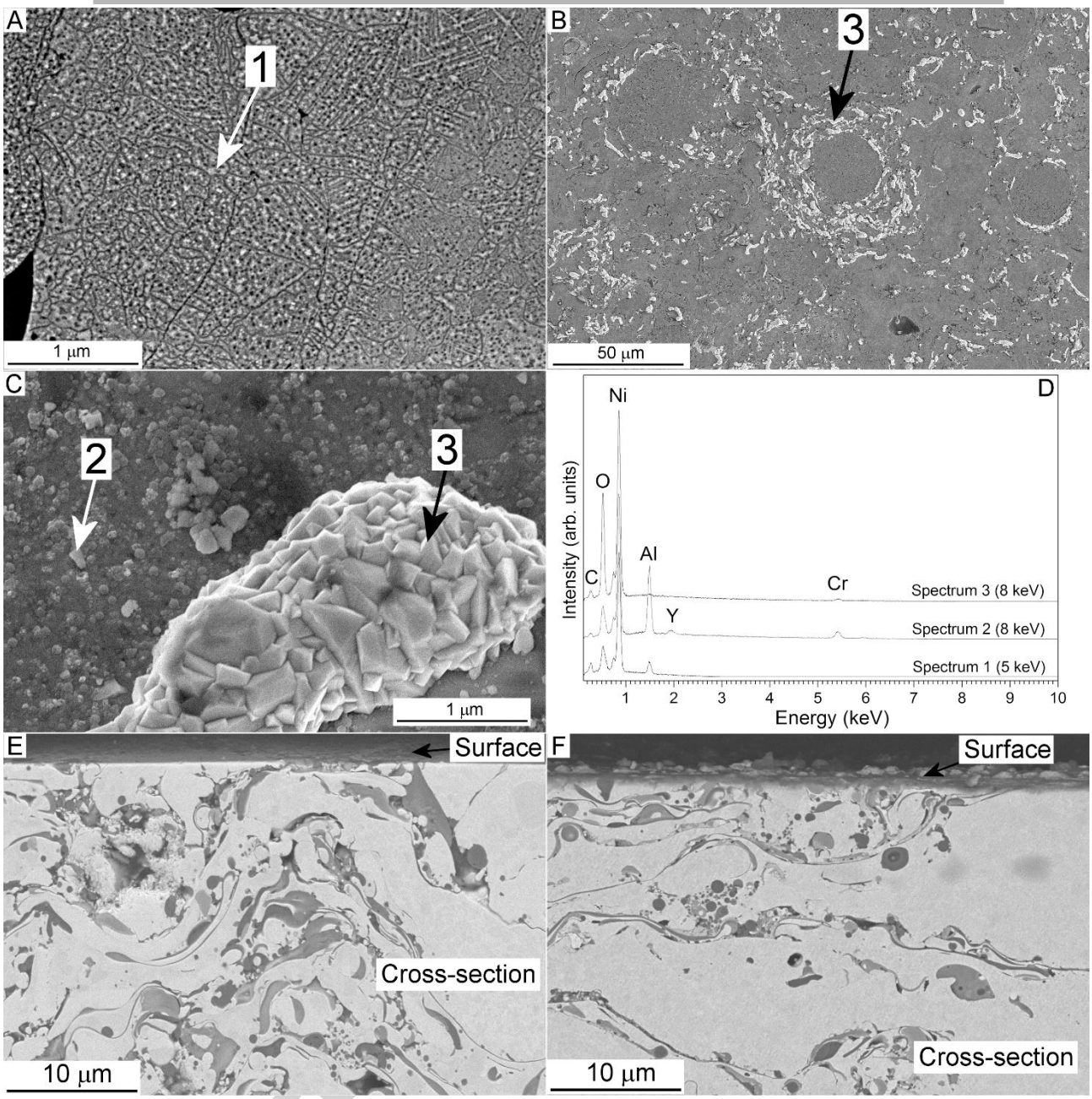

Figure 17. FEG-SEM micrographs of the oxidised surface of the samples outside the wear scars, after ball-on-disk testing at 400 °C (A) and at 700 °C (B,C), with EDX spectra (D) acquired at locations 1-3 marked on the micrographs, and corresponding cross-sections (E: 400 °C, F: 700 °C).

(ii) The generation of lattice defects in the metal by plastic deformation near the contact surface. Accordingly, plastic shearing and delamination (sometimes following interlamellar boundaries) occur wherever spallation of the oxide layer leaves the coating surface uncovered, which is seen particularly at 400 °C (Fig. 18), consistent with the higher wear

rates recorded at this temperature compared to those at 700 °C (Fig. 10). Such defects indeed favour oxygen diffusion and allow faster oxidation rate.

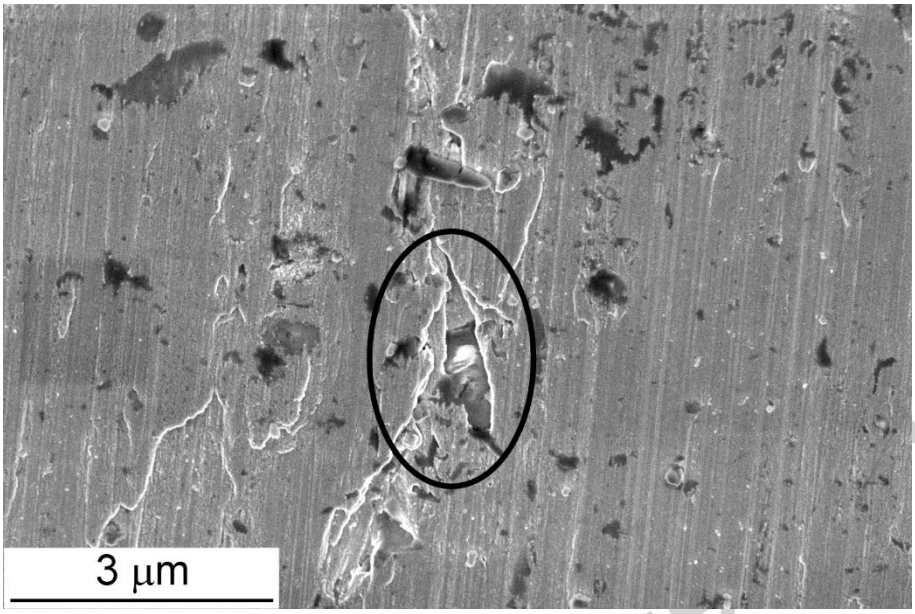

Figure 18. FEG-SEM detail of the worn surface of the NiCrAlY+3%Al_2O_3 sample after wear testing at 400 °C. The circled area indicates metal delamination in an uncovered area.

However, unlike bulk metals, where the "glaze" often exhibits a layered structure due to complex cation and anion diffusion phenomena across the oxide scale [65,69], the present "glaze" is a uniform mixture of $NiAl_2O_4$- and $NiCr_2O_4$-type spinel oxides (Fig. 15A), comprising all of the alloy elements (Fig. 15B). The embedded Al_2O_3 reinforcement is also seen through the fluorescence peak at about 1410 cm^{-1} (Fig. 15A) [70]. It is inferred that the entire NiCrAlY alloy was oxidised at some locations, while it remained unaffected at others (the mentioned metal stripes – Fig. 14, label "1"). This probably follows from the action of one more mechanism, peculiar to thermally sprayed coatings only. Specifically, air can penetrate the splat-boundary defects (e.g. gaps and micro-cracked oxide stringers, Section 3.1), which are further enlarged by the surface stresses under sliding contact conditions. This, together with mechanisms (i) and (ii) above, causes fast interaction of the exposed metal with oxygen, whilst some areas in the core of the splats remain unreacted to yield the scale morphology seen in Fig. 14E-H.

3.4.4 Overall considerations on the effect of Al_2O_3 reinforcement

At high temperatures, oxidation of the NiCrAlY matrix takes on the role that the pulled-out Al_2O_3 particles had at room temperature: it is possible to state that the NiCrAlY matrix can "self-protect" itself against adhesive wear at high temperature. Since the NiCrAlY matrix contributes a much larger fraction of the coating surface than that occupied by the Al_2O_3 particles, and since the latter are surmounted by the "glaze" layer, their role becomes marginal, explaining the performance levelling seen in Fig. 10.

For pure NiCrAlY, in particular, such self-protection causes a significant decrease of the wear rate from room temperature to 400 °C, due to the change in the dominant wear mechanism from adhesion to tribo-oxidation. The composite coatings with the highest Al_2O_3 contents, on the other hand, were already capable of protecting themselves by tribo-oxidation at room temperature, so there is no beneficial effect for these samples at 400 °C. Their wear rate even increases, probably because the "glaze" film is less stable at 400 °C than it is at 700 °C, which is revealed by the residual occurrence of some adhesive/delaminative wear (Fig. 18). Moreover, the hardness of the system at 700 °C, though certainly not the same as that measured at room temperature in Fig. 9A, does benefit from the improved interlamellar cohesion and from the precipitation of the β-phase as discussed in Section 3.3. Both phenomena can indeed restrain the adhesion of the uncovered NiCrAlY areas to the mating surface and the consequent delamination. A comparable wear resistance enhancement due to high-temperature strength increase was accordingly observed for a Ni-Al intermetallic [71].

At 400 °C, an oxidised tribofilm also covers the counterbody surface (Fig. 12H), similar to the room temperature behaviour (Fig. 12D,F), but the average friction coefficient is lower (Fig. 10B), probably because the adhesion and interlocking between the tribo-layers on the mating surfaces decrease. The intrinsically different nature of the smooth "glaze" formed on the coating at 400 °C, and the absence of adsorbed humidity at this temperature, may account for this fact. At 700 °C, to the contrary, most of the wear scar on the counterbody is free of tribolayers. Some individual grains

of the sintered Al_2O_3 ball can indeed be recognised on the wear surface, which bears evidence of mild polishing and of irregular grooving (Fig. 12L). The lack of a transfer layer may be the cause for the further decrease of the friction coefficient, compared to the 400 °C condition (Fig. 10B).

4. Conclusions

A "hybrid" atmospheric plasma spray process with dual-injection system was employed to produce NiCrAlY+Al_2O_3 composite coatings for sliding wear protection of mechanical components over a wide range of temperatures. Conventional feeding of the NiCrAlY powder in dry form was coupled to the injection of a suspension of fine Al_2O_3 particles dispersed in ethanol.

The following conclusions can be drawn from the experimental results listed above:

- The coatings consist of large NiCrAlY lamellae interspersed with fine, rounded Al_2O_3 particles. Spraying in air caused some oxidation along the lamellar boundaries of the NiCrAlY phase, decreasing the interlamellar cohesive strength, and depriving the metal alloy of its most reactive elements (namely Al and Y).
- The addition of Al_2O_3 particles only causes marginal changes in hardness.
- The addition of Al_2O_3 causes room-temperature sliding wear rates to decrease monotonically from $\approx 5*10^{-4}$ $mm^3/(Nm)$ for pure NiCrAlY to $\approx 5*10^{-6}$ $mm^3/(Nm)$ for NiCrAlY+18wt.% Al_2O_3. Pure NiCrAlY suffers from severe adhesive/delaminative wear, favoured by the presence of brittle interlamellar oxide inclusions.

  In the composite coatings, the wear mechanisms changes to tribo-oxidation with minor occurrence of adhesion. The pull-out of some Al_2O_3 particles is the key factor to initiate the formation of a tribo-layer, which progressively evolves through the smearing and compaction of oxidised NiCrAlY fragments. Wear proceeds by local cracking and spallation of the tribo-layer, allowing for the occasional occurrence of adhesive wear.

- At 400 °C and at 700 °C, the wear rates of all samples are levelled to ≈$8*10^{-5}$ mm^3/(Nm) and ≈$2*10^{-5}$ mm^3/(Nm) respectively.

  The dominant wear mechanism is tribo-oxidation, but, in this case, it proceeds through direct oxidation of the coating surface to develop a dense "glaze" layer. The effect of the added Al_2O_3 therefore becomes irrelevant.

  Additional changes to the NiCrAlY matrix occurring at 700 °C (partial healing of the interlamellar boundaries and intra-lamellar re-precipitation of sub-micrometric β-NiAl phase) further help reducing the occurrence of adhesive wear in uncovered areas. This, together with the better stability of the "glaze" layer at this temperature, explains why the wear rate at 700 °C is lower than that at 400 °C.

References

[1] J.R. Davis, Handbook of Thermal Spray Technology, ASM International, Materials Park, OH, USA, 2004.

[2] B.S. Mann, B. Prakash, High temperature friction and wear characteristics of various coating materials for steam valve spindle application, Wear 240 (2000) 223–230.

[3] R.N. Johnson, Wear resistant coatings for reactor components in liquid sodium environments, J. Vac. Sci. Technol. 11 (1974) 759.

[4] C.C. Li, Characterization of thermally sprayed coatings for high temperature wear protection applications, Thin Solid Films 73 (1980) 59–77.

[5] W.J. Bryan, D. Jones, Wear resistant coating for components of fuel assemblies and control assemblies, and method of enhancing wear resistance of fuel assembly and control assembly components using wear-resistant coating - US Patent, 5,434,896, 1995.

[6] S. Matthews, B. James, M. Hyland, High temperature erosion-oxidation of Cr_3C_2-NiCr thermal spray coatings under simulated turbine conditions, Corros. Sci. 70 (2013) 203–211.

[7] S. Bose, High Temperature Coatings, Butterworth-Heinemann, Oxford, UK, 2007.

[8] J.A. Cabral-Miramontes, C. Gaona-Tiburcio, F. Almeraya-Calderón, F.H. Estupiñan-Lopez, G.K. Pedraza-Basulto, C.A. Poblano-Salas, Parameter Studies on High-Velocity Oxy-Fuel Spraying of CoNiCrAlY Coatings Used in the Aeronautical Industry, Int. J. Corros. 2014 (2014) 1–8.

[9] S. Li, C. Langlade, S. Fayeulle, D. Trkheux, Influence of the microstructure of plasma deposited MCrAlY their tribological behaviour, Surf. Coat. Technol. 101 (1998) 7–11.

[10] P. Colomban, S. Jullian, M. Parlier, P. Monge-Cadet, Identification of the high-temperature impact/friction of aeroengine blades and cases by micro Raman spectroscopy, Aerosp. Sci. Technol. 3 (1999) 447–459.

[11] H. Wang, D. Zuo, M. Wang, G. Sun, H. Miao, Y. Sun, High temperature frictional wear behaviors of nano-particle reinforced NiCoCrAlY cladded coatings, Trans. Nonferrous Met. Soc. China 21 (2011) 1322–1328.

[12] K. Bobzin, T. Schläfer, K. Richardt, M. Brühl, Development of Oxide Dispersion Strengthened MCrAlY Coatings, J. Therm. Spray Technol. 17 (2008) 853–857.

[13] L. Zhao, M. Parco, E. Lugscheider, Wear behaviour of Al_2O_3 dispersion strengthened MCrAlY coating, Surf. Coat. Technol. 184 (2004) 298–306.

[14] Y. Cao, C. Huang, W. Liu, W. Zhang, L. Du, Effects of Boron Carbide Content on the Microstructure and Properties of Atmospheric Plasma-Sprayed NiCoCrAlY/Al_2O_3-B_4C Composite Coatings, J. Therm. Spray Technol. 23 (2014) 716–724.

[15] D.E. Crawmer, Coating Structures, Properties, and Materials, in: J.R. Davis (Ed.), Handb. Therm. Spray Technol., ASM International, Materials Park, OH, USA, 2004: pp. 47–53.

[16] M. Okada, R. Vassen, M. Karger, D. Sebold, D. Mack, M.O. Jarligo, et al., Deposition and oxidation of oxide-dispersed CoNiCrAlY bondcoats, J. Therm. Spray Technol. 23 (2014) 147–153.

[17] F. Bozza, Protezione di componenti per la produzione di energia attraverso tecniche di ingegneria delle superfici: sviluppo di bondcoat rinforzati tramite dispersione di ossidi e coating diffusivi a base cromo (Protection of energy production components through surface engineering techniques: development of oxide dispersion strengthened bondcoats and of chromium-based diffusion coatings), Ph.D. Thesis, University of Modena and Reggio Emilia, Italy, 2013.

[18] P. Fauchais, G. Montavon, R.S. Lima, B.R. Marple, Engineering a new class of thermal spray nano-based microstructures from agglomerated nanostructured particles, suspensions

and solutions: an invited review, J. Phys. D. Appl. Phys. 44 (2011) 093001.

[19] P. Fauchais, R. Etchart-Salas, V. Rat, J.F. Coudert, N. Caron, K. Wittmann-Ténèze, Parameters Controlling Liquid Plasma Spraying: Solutions, Sols, or Suspensions, J. Therm. Spray Technol. 17 (2008) 31–59.

[20] J. Fazilleau, C. Delbos, V. Rat, J.F. Coudert, P. Fauchais, B. Pateyron, Phenomena Involved in Suspension Plasma Spraying Part 1: Suspension Injection and Behavior, Plasma Chem. Plasma Process. 26 (2006) 371–391.

[21] P. Fauchais, V. Rat, C. Delbos, J.F. Coudert, T. Chartier, L. Bianchi, Understanding of suspension DC plasma spraying of finely structured coatings for SOFC, IEEE Trans. Plasma Sci. 33 (2005) 920–930.

[22] F. Cipri, F. Marra, G. Pulci, J. Tirillò, C. Bartuli, T. Valente, Plasma sprayed composite coatings obtained by liquid injection of secondary phases, Surf. Coat. Technol. 203 (2009) 2116–2124.

[23] G. Bertolissi, C. Chazelas, G. Bolelli, L. Lusvarghi, M. Vardelle, A. Vardelle, Engineering the microstructure of solution precursor plasma-sprayed coatings, J. Therm. Spray Technol. 21 (2012) 1148–1162.

[24] G. Hou, Y. An, X. Zhao, H. Zhou, J. Chen, Effect of alumina dispersion on oxidation behavior as well as friction and wear behavior of HVOF-sprayed CoCrAlYTaCSi coating at elevated temperature up to 1000 °C, Acta Mater. 95 (2015) 164–175.

[25] J. Chen, Y. An, J. Yang, X. Zhao, F. Yan, H. Zhou, et al., Tribological properties of adaptive NiCrAlY–Ag–Mo coatings prepared by atmospheric plasma spraying, Surf. Coat. Technol. 235 (2013) 521–528.

[26] J. Nohava, B. Bonferroni, G. Bolelli, L. Lusvarghi, Interesting aspects of indentation and scratch methods for characterization of thermally-sprayed coatings, Surf. Coat. Technol. 205 (2010) 1127–1131.

[27] W. Oliver, G. Pharr, An improved technique for determining hardness and elastic modulus using load and displacement-sensing indentation systems, J. Mater. Res. 7 (1992) 1564–1583.

[28] P. Poza, J. Gómez-García, C.J. Múnez, TEM analysis of the microstructure of thermal barrier coatings after isothermal oxidation, Acta Mater. 60 (2012) 7197–7206.

[29] S. Deshpande, S. Sampath, H. Zhang, Mechanisms of oxidation and its role in microstructural evolution of metallic thermal spray coatings - Case study for Ni-Al, Surf.

Coat. Technol. 200 (2006) 5395–5406.

[30] P. Richer, M. Yandouzi, L. Beauvais, B. Jodoin, Oxidation behaviour of CoNiCrAlY bond coats produced by plasma, HVOF and cold gas dynamic spraying, Surf. Coat. Technol. 204 (2010) 3962–3974.

[31] V. Higuero, F.J. Belzunce, J. Riba, High temperature oxidation of plasma and hvof thermal sprayed CoNiCrAlY coatings in simulated gas turbine and furnace environments, Surf. Eng. 25 (2009) 319–325.

[32] W.R. Chen, X. Wu, B.R. Marple, D.R. Nagy, P.C. Patnaik, TGO growth behaviour in TBCs with APS and HVOF bond coats, Surf. Coat. Technol. 202 (2008) 2677–2683.

[33] M. Shibata, S. Kuroda, H. Murakami, M. Ode, M. Watanabe, Y. Sakamoto, Comparison of Microstructure and Oxidation Behavior of CoNiCrAlY Bond Coatings Prepared by Different Thermal Spray Processes, Mater. Trans. 47(7) (2006) 1638–1642.

[34] B.M. Cetegen, S. Basu, Review of Modeling of Liquid Precursor Droplets and Particles Injected into Plasmas and High-Velocity Oxy-Fuel (HVOF) Flame Jets for Thermal Spray Deposition Applications, J. Therm. Spray Technol. 18 (2009) 769–793.

[35] H.-B. Xiong, J.-Z. Lin, Nanoparticles Modeling in Axially Injection Suspension Plasma Spray of Zirconia and Alumina Ceramics, J. Therm. Spray Technol. 18 (2009) 887–895.

[36] B. Pateyron, L. Pawłowski, N. Calve, G. Delluc, A. Denoirjean, Modeling of phenomena occurring in plasma jet during suspension spraying of hydroxyapatite coatings, Surf. Coat. Technol. 214 (2013) 86–90.

[37] K. VanEvery, M.J.M. Krane, R.W. Trice, H. Wang, W. Porter, M. Besser, et al., Column Formation in Suspension Plasma-Sprayed Coatings and Resultant Thermal Properties, J. Therm. Spray Technol. 20 (2011) 817–828.

[38] M. Di Ferdinando, A. Fossati, A. Lavacchi, U. Bardi, F. Borgioli, C. Borri, et al., Isothermal oxidation resistance comparison between air plasma sprayed, vacuum plasma sprayed and high velocity oxygen fuel sprayed CoNiCrAlY bond coats, Surf. Coat. Technol. 204 (2010) 2499–2503.

[39] R. McPherson, On the formation of thermally sprayed alumina coatings, J. Mater. Sci. 15 (1980) 3141–3149.

[40] K. Sabiruddin, J. Joardar, P.P. Bandyopadhyay, Analysis of phase transformation in plasma sprayed alumina coatings using Rietveld refinement, Surf. Coat. Technol. 204 (2010) 3248–3253.

[41] J. Song, K. Ma, Y. Li, L. Zhang, J.M. Schoenung, High temperature microstructure and microhardness evolution in dense NiCrAlY bulk material fabricated by spark plasma sintering, Mater. Sci. Eng. A. 528 (2011) 3210–3217.

[42] G. Bolelli, V. Cannillo, L. Lusvarghi, F.P. Mantini, E. Gualtieri, C. Menozzi, An FIB study of sharp indentation testing on plasma-sprayed TiO_2, Mater. Lett. 62 (2008) 1557–1560.

[43] G. Di Girolamo, M. Alfano, L. Pagnotta, A. Taurino, J. Zekonyte, R.J.K. Wood, On the Early Stage Isothermal Oxidation of APS CoNiCrAlY Coatings, J. Mater. Eng. Perform. 21 (2012) 1989–1997.

[44] J.-Y. Kwon, J.-H. Lee, Y.-G. Jung, U. Paik, Effect of bond coat nature and thickness on mechanical characteristic and contact damage of zirconia-based thermal barrier coatings, Surf. Coat. Technol. 201 (2006) 3483–3490.

[45] H. Waki, T. Kitamura, A. Kobayashi, Effect of Thermal Treatment on High-Temperature Mechanical Properties Enhancement in LPPS, HVOF, and APS CoNiCrAlY Coatings, J. Therm. Spray Technol. 18 (2009) 500–509.

[46] H. Waki, K. Ogura, I. Nishikawa, A. Ohmori, Monotonic and cyclic deformation behavior of plasma-sprayed coatings under uni-axial compressive loading, Mater. Sci. Eng. A. 374 (2004) 129–136.

[47] G. Bolelli, B. Bonferroni, J. Laurila, L. Lusvarghi, A. Milanti, K. Niemi, et al., Micromechanical properties and sliding wear behaviour of HVOF-sprayed Fe-based alloy coatings, Wear 276-277 (2012) 29–47.

[48] G. Bolelli, A. Milanti, L. Lusvarghi, L. Trombi, H. Koivuluoto, P. Vuoristo, Wear and impact behaviour of High Velocity Air-Fuel sprayed Fe-Cr-Ni-B-C alloy coatings, Tribol. Int. (submitted).

[49] G. Bolelli, Tribology of metallic and hardmetal thermal spray coatings at high temperature, in: Proceedings of the Workshop on Thermal Spray and Laser Clad Coatings - Coatings for High Temperature Applications, Plzeň, Czech Republic, 2014.

[50] J. Pereira, J. Zambrano, M. Licausi, M. Tobar, V. Amigó, Tribology and high temperature friction wear behavior of MCrAlY laser cladding coatings on stainless steel, Wear 330-331 (2015) 280–287.

[51] W.A. Glaeser, Wear Debris Classification, in: B. Bhushan (Ed.), Modern Tribology Handbook – Vol. 1, CRC Press, Boca Raton, FL, USA, 2001: pp. 301–315.

[52] A. Edrisy, A.T. Alpas, T. Perry, Wear mechanism maps for thermal-spray steel coatings, Metall. Mater. Trans. A. 36 (2005) 2737–2750.

[53] L. Ceschini, A. Marconi, C. Martini, A. Morri, Tribological behavior of components for radial piston hydraulic motors: Bench tests, failure analysis and laboratory dry sliding tests, Wear 305 (2013) 238–247.

[54] G.W. Stachowiak, A.W. Batchelor, Engineering Tribology, Third Edition, Elsevier Butterworth-Heinemann, Burlington, MA, USA, MA, USA, 2005.

[55] J. Jiang, F.H. Stott, M.M. Stack, A generic model for dry sliding wear of metals at elevated temperatures, Wear 256 (2004) 973–985.

[56] J. Jiang, F.H. Stott, M.M. Stack, The role of triboparticulates in dry sliding wear, Tribol. Int. 31 (1998) 245–256.

[57] G. Straffelini, Wear mechanisms, in: Friction and Wear - Methodologies for Design and Control, Springer International Publishing AG, Cham, Switzerland, Switzerland, 2015: pp. 85–113.

[58] M.A. Laguna-Bercero, M.L. Sanjuán, R.I. Merino, Raman spectroscopic study of cation disorder in poly- and single crystals of the nickel aluminate spinel., J. Phys. Condens. Matter. 19 (2007) 186217.

[59] Z. Wang, S.K. Saxena, P. Lazor, H.S.C. O'Neill, An in situ Raman spectroscopic study of pressure induced dissociation of spinel $NiCr_2O_4$, J. Phys. Chem. Solids 64 (2003) 425–431.

[60] G. Gouadec, P. Colomban, Raman Spectroscopy of nanomaterials: How spectra relate to disorder, particle size and mechanical properties, Prog. Cryst. Growth Charact. Mater. 53 (2007) 1–56.

[61] J. Jiang, F.H. Stott, M.M. Stack, A mathematical model for sliding wear of metal at elevated temperatures, Wear 181-183 (1995) 20–31.

[62] F.H. Stott, D.S. Lin, G.C. Wood, The structure and mechanism of formation of the "glaze" oxide layers produced on nickel-based alloys during wear at high temperatures, Corros. Sci. 13 (1973) 449–469.

[63] F.H. Stott, J. Glascott, G.C. Wood, Factors affecting the progressive development of wear-protective oxides on iron-base alloys during sliding at elevated temperatures, Wear 97 (1984) 93–106.

[64] W.R. Chen, X. Wu, B.R. Marple, P.C. Patnaik, Oxidation and crack nucleation/growth in an air-plasma-sprayed thermal barrier coating with NiCrAlY bond coat, Surf. Coat. Technol. 197 (2005) 109–115.

[65] P.D. Wood, H.E. Evans, C.B. Ponton, Investigation into the wear behaviour of Tribaloy 400C during rotation as an unlubricated bearing at 600°C, Wear. 269 (2010) 763–769.

[66] K. Nakayama, H. Hashimoto, Triboemission from various materials in atmosphere, Wear 47 (1991) 335–343.

[67] K. Nakayama, Tribochemical Reaction, and Friction and Wear in Ceramics Under Various N- Butane Gas Pressures, Tribol. Int. 29 (1996) 385/393.

[68] C.K. Kajdas, Importance of the triboemission process for tribochemical reaction, Tribol. Int. 38 (2005) 337–353.

[69] P.D. Wood, H.E. Evans, C.B. Ponton, Investigation into the wear behaviour of Stellite 6 during rotation as an unlubricated bearing at 600°C, Tribol. Int. 44 (2011) 1589–1597.

[70] G. Gouadec, P. Colomban, N. Piquet, M.F. Trichet, L. Mazerolles, Raman/Cr^{3+} fluorescence mapping of a melt-grown $Al_2O_3/GdAlO_3$ eutectic, J. Eur. Ceram. Soc. 25 (2005) 1447–1453.

[71] P.J. Blau, Elevated-temperature tribology of metallic materials, Tribol. Int. 43 (2010) 1203–1208.

Highlights

NiCrAlY+Al_2O_3 composite coatings were produced by dual-injection plasma spray

Dry NiCrAlY powders were fed together with fine Al_2O_3 particles dispersed in ethanol

Large NiCrAlY lamellae are interspersed with fine, rounded Al_2O_3 particles

Room-temperature sliding wear rates drop by 2 orders of magnitude with Al_2O_3 addition

At 400 and 700 °C, tribo-oxidation levels all wear rates regardless of Al_2O_3 content